National Research FLAGSHIPS
Water for a Healthy Country

CSIRO

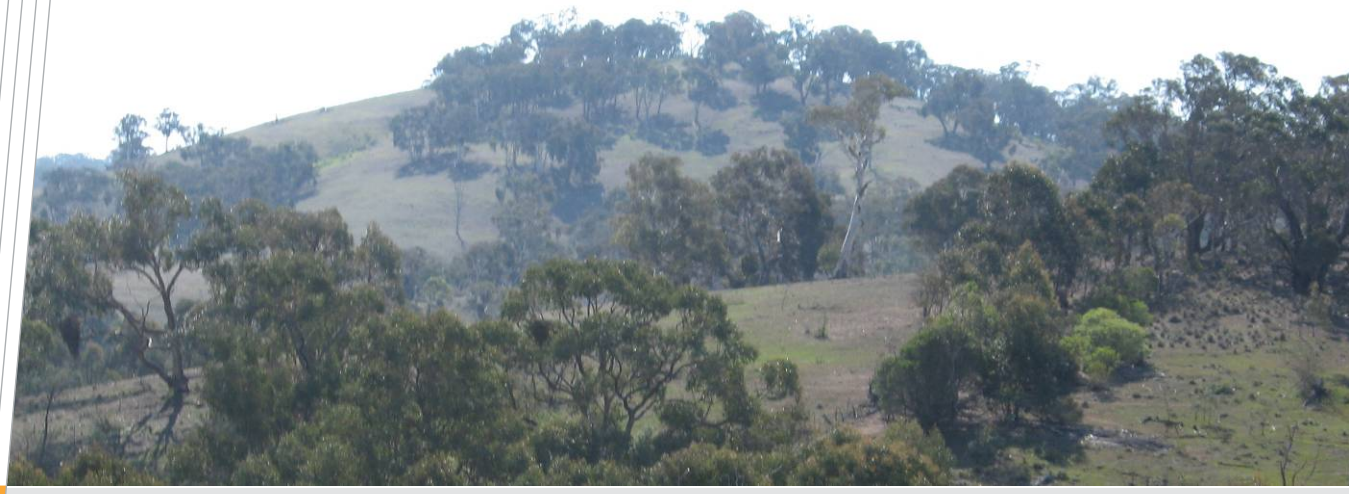

www.csiro.au

The Australian Water Resources Assessment System

Technical Report 3. Landscape Model (version 0.5) Technical Description

AIJM Van Dijk

17 June 2010

A water information R & D alliance between the Bureau of Meteorology and CSIRO's Water for a Healthy Country Flagship

Australian Government
Bureau of Meteorology

Water Information
DATA › INFORMATION › INSIGHT

Water for a Healthy Country Flagship Report series ISSN: 1835-095X

Australia is founding its future on science and innovation. Its national science agency, CSIRO, is a powerhouse of ideas, technologies and skills.

CSIRO initiated the National Research Flagships to address Australia's major research challenges and opportunities. They apply large scale, long term, multidisciplinary science and aim for widespread adoption of solutions. The Flagship Collaboration Fund supports the best and brightest researchers to address these complex challenges through partnerships between CSIRO, universities, research agencies and industry.

The Water for a Healthy Country Flagship aims to provide Australia with solutions for water resource management, creating economic gains of $3 billion per annum by 2030, while protecting or restoring our major water ecosystems.

The work contained in this report is collaboration between CSIRO's Water for a Healthy Country Flagship and the Bureau of Meteorology's Water Division under the Water Information Research and Development Alliance (WIRADA).

WIRADA is a five-year, $50 million partnership that will use CSIRO's R&D expertise to help the Bureau of Meteorology report on availability, condition and use of Australia's water resources.

For more information about the partnership visit www.csiro.au/partnerships/WIRADA.html

For more information about Water for a Healthy Country Flagship or the National Research Flagship Initiative visit www.csiro.au/org/HealthyCountry.html

Citation: Van Dijk, A. I. J. M. 2010. The Australian Water Resources Assessment System. Technical Report 3. Landscape Model (version 0.5) Technical Description. CSIRO: Water for a Healthy Country National Research Flagship.

Copyright and Disclaimer

Important Disclaimer:

Cover Photo: Description: Some Paddock trees on Bywong Hill, Palerang, NSW © 2009 AIJM Van Dijk. File: BywongHill.jpg

ABOUT THIS REPORT

Through the Water Information Research and Development Alliance, the Bureau of Meteorology and CSIRO are developing the Australian water resources assessment system (AWRA). The AWRA system is integrated software that combines hydrological models with a variety of observations and observation-derived products.

The purpose of the AWRA system is to operationally provide up to date, credible, comprehensive, accurate and relevant information about the history, present state and future trajectory of the water balance, with sufficient detail to inform water resources management. Intended dissemination of the information is through the Bureau's water information services, in particular, occasional and scheduled water resources assessments and the annual National Water Account.

The technical details and evaluation of the AWRA system are documented in a series of reports that are updated as new system or component versions are developed. Reports in this series are (the current report is highlighted):

- 1. System Conceptual Design
- 2. Implementation Document
- **3. Landscape Model (version 0.5) Technical Description**
- 4. Landscape Model (version 0.5) Evaluation Against Observations

EXECUTIVE SUMMARY

This report is one of a series on the Australian Water Resources Assessment system (AWRA), and provides a technical description of the AWRA Landscape Model (AWRA-L, version 0.5). The model aims to produce interpretable water balance component estimates, and as much as possible agree with relevant on-ground and satellite observations, which will be considered for model calibration and model-data assimilation.

AWRA-L (version 0.5) has the following characteristics:

- Grid-based structure: the model can be applied at any resolution; current implementation is at 0.05° to be commensurate with the resolution of available meteorological data.
- Flexible number of hydrological response units (HRUs) in each grid cell. Currently 2 HRUs are considered; tall, deep-rooted vegetation and short, shallow-rooted vegetation.
- For each HRU, the water balance of the topsoil, shallow soil and deep soil are simulated, as well as leaf biomass. Groundwater and surface water dynamics are simulated at grid resolution; effectively taking each grid cell to represent a (number of identical) catchment(s).
- Where available, simple and established equations are used to describe processes determining the radiation, energy and water balance. New approaches needed to be developed to describe surface albedo dynamics and vegetation phenology (that is, seasonal canopy dynamics), and a simplified form of Richard's equation was derived to describe soil water drainage.
- All HRU and catchment parameters can be prescribed as uniform values or as spatially varying grids. Suggested values are provided for all parameters based on literature review or analyses carried out as part of model development.
- Minimum meteorological inputs are daily gridded estimates of precipitation, incoming short-wave radiation, and daytime temperature (currently estimated from minimum and maximum temperature). Where wind speed, vapour pressure and air pressure data are available, they can be used.

An important caveat for the current model version is the assumption that lateral redistribution between grid cells can be ignored. This is an area of ongoing development and needs to be considered when interpreting the results for areas that may be subject to irrigation, inundation or groundwater inflows.

All model equations are listed and explained in this report, organised into sections pertaining to the movement of liquid water (Section 2), the surface energy balance and potential ET (Section 3), the evaporative or vapour fluxes (Section 4), and the algorithms used to describe vegetation phenology (Section 5). Each section discusses all balance equations; unit conversion equations; and process equations to estimate the individual terms in the balance equations. For each process equation, the variables and parameters that are associated with it are listed, followed by a rationale explaining why the equation was chosen in favour of any alternatives or how it was developed, and a brief discussion on the range of values for any parameters in the equation. The code of the MATLAB™ version of the AWRA-L (version 0.5 time step) is provided as an appendix.

The model is recommended as suitable for the production of regular water resource assessments and water accounts, but opportunities for further development are identified.

CONTENTS

ACKNOWLEDGEMENTS

This report has benefit greatly from discussions with and/or reviews from Andrew Frost, David Barratt, Sri Srikanthan and Elisabetta Carrara (all Bureau of Meteorology, Water Division); Tim McVicar, Warrick Dawes, Francis Chiew, Zahra Paydar, Jamie Vleeshouwer, Randall Donohue, Juan Pablo Guerschman and Brian Smerdon (all CSIRO Land and Water); and Ray Leuning (CSIRO Marine and Atmospheric Research). Their input is gratefully acknowledged.

LIST OF ACRONYMS

ASAR GM	advanced synthetic aperture radar, operated in global monitoring mode
AMEP	annual mean excess precipitation
AVHRR	advanced very high resolution radiometer
AWRA	Australian Water Resources Assessment system
AWRA-L	AWRA Landscape model
BAWAP	Bureau of Meteorology component of Australian Water Availability Project
CBL	convective boundary layer
CSIRO	Commonwealth Scientific and Industrial Research Organisation
ESMA	explicit soil moisture accounting
ET	evapotranspiration
EVI	enhanced vegetation index
FAO	Food and Agricultural Organisation
FPAR	absorbed fraction photosynthetically active radiation
HRU	hydrological response unit
IDE	inflow dependent ecosystem
LAI	leaf area index
MAP	mean annual precipitation
MODIS	moderate resolution imaging spectrometer
NDVI	normalised difference vegetation index
NWP	numerical weather prediction
PCI	photosynthetic capacity index
PET	potential evapotranspiration
P-M	Penman-Monteith (equation)
P-T	Priestley-Taylor (equation)
RAD	incoming shortwave radiation
TMIN	daily minimum temperature
TMAX	daily maximum temeprature
VP09	vapour pressure at 9:00 am
VP15	vapour pressure at 15:00 pm

LIST OF SYMBOLS

Roman symbols

A_n	daytime net available energy (W m^{-2})
C_{SLA}	specific leaf area per unit dry leaf biomass (m^2 kg^{-1})
C_{TR}	coefficient to estimate outgoing longwave radiation from air temperature (W m^{-2} K^{-4})
c_{RE}	unit conversion from latent heat flux to potential evaporation (mm m^2 d^{-1} W^{-1})
D_0	top soil water drainage (mm d^{-1})
D_d	deep soil water drainage (mm d^{-1})
D_g	ground water drainage (mm d^{-1})
D_s	shallow soil water drainage (mm d^{-1})
E_0	potential evapotranspiration (mm d^{-1})
E_e	combined evaporation (mm d^{-1})
E_g	groundwater evaporation (mm d^{-1})
E_i	interception evaporation (mm d^{-1})
E_r	surface water evaporation (mm d^{-1})
E_s	soil evaporation (mm d^{-1})
E_t	transpiration (mm d^{-1})
F_{dg}	factor describing connectivity between soil and groundwater (-)
F_{ER0}	average ratio of wet canopy evaporation rate and rainfall rate for full canopy cover (-)
$F_{loss,max}$	maximum fraction of daytime net radiation 'lost' to heat storage when there is no vegetation (-)
F_{OW}	open water evaporation scaling factor (-)
$F_{S,ref}$	reference soil cover fraction that determines the rate of decline in energy loss with increasing canopy cover (-)
f_{drain}	daily drainage fraction (-)
f_{day}	fraction daylight hours (-)
f_{ER}	estimated ratio of wet canopy evaporation rate and rainfall rate (-)
f_{RH}	relative humidity (-)
f_S	fraction uncovered surface (-)
f_{sat}	fraction area saturated (-)
f_{sE}	soil evaporation fraction (-)
f_{sEmax}	maximum soil evaporation fraction (-)
f_t	transpiration fraction (-)
f_V	vegetation canopy cover (-)
$f_{V,max}$	maximum achievable canopy cover (-)
f_{Veq}	equilibrium canopy cover (-)
f_{water}	fraction covered by water (-)
G_{smax}	maximum surface conductance for closed canopy (m s^{-1})
g_a	aerodynamic conductance (m s^{-1})
g_s	maximum surface conductance (m s^{-1})
H	climate wetness
h	vegetation canopy height (m)
I	infiltration (mm d^{-1})
I_0	initial retention capacity (mm)
I_i	initial infiltration (mm)
K_{FC}	daily drainage fraction at field capacity (-)
K_g	groundwater drainage coefficient (-)
K_r	streamflow drainage coefficient ()
k_{u2}	coefficient relating climate station wind speed at 2 m height to aerodynamic conductance (-)
k_α	coefficient analogous to Priestley-Taylor coefficient (-)
k_e	coefficient determining the efficiency of energy use for evaporation (-)
M_L	dry leaf biomass per unit area (kg m^{-2})
M_{Leq}	equilibrium dry leaf biomass (kg m^{-2})
m_{Ln}	net rate of change in leaf biomass per unit area (kg m^{-2} d^{-1})
P_g	gross precipitation (mm d^{-1})
P_n	net precipitation (mm d^{-1})
P_{ref}	reference event precipitation for runoff generation (mm d^{-1})
P_{wet}	precipitation needed to saturate canopy (mm d^{-1})
p_{air}	air pressure (Pa)
p_e	vapour pressure (Pa)
p_{es}	saturated vapour pressure (Pa)
Q	streamflow (mm d^{-1})
Q_R	surface runoff (mm d^{-1})

R_{Lin}	incoming longwave radiation (W m^{-2})
R_{loss}	radiation energy 'lost' to heat storage and photosynthesis (W m^{-2})
R_{Lout}	outgoing longwave radiation (W m^{-2})
R_n	net radiation (W m^{-2})
R_{Sin}	incoming shortwave radiation (W m^{-2})
R_{Sn}	net shortwave radiation (W m^{-2})
R_{Ln}	net longwave radiation (W m^{-2})
R_{Sout}	outgoing shortwave radiation (W m^{-2})
S_0	top soil water storage (mm)
S_d	deep soil water storage (mm)
S_{FC}	soil water storage at field capacity ()
S_g	groundwater storage (mm)
S_{Gref}	reference groundwater storage for saturated fraction estimation (mm)
S_r	runoff storage (mm)
S_s	shallow soil water storage (mm)
S_V	canopy rainfall storage capacity (mm)
s_V	canopy storage capacity per unit leaf area (mm)
S_{zFC}	accessible soil water storage at field capacity of layer z (mm)
T_{a*}	effective air temperature (°C)
t_{grow}	time constant determining rate of canopy increase (d)
$t_{senesce}$	time constant determining rate of canopy decrease (d)
U_0	maximum root water uptake (mm d^{-1})
U_{0z}	maximum root water uptake from layer z (mm d^{-1})
U_z	root water uptake from layer z (mm d^{-1})
u_{*2}	effective wind speed at 2 m (m s^{-1})
u_2	wind speed at 2 m (m s^{-1})
w_{0lim}	relative water content of top soil at which evaporation is reduced (-)
w_z	relative wetness of layer z (-)
w_{zlim}	relative water content of layer z at which root uptake is reduced (-)
$w_{\alpha,ref}$	reference value of w_0 describing the relationship between albedo and top soil wetness (-)
Y	capillary rise, from groundwater to deep soil (mm d^{-1})

Greek symbols

α_{dry}	dry soil albedo (-)
α_S	soil albedo (-)
α_V	vegetation albedo (-)
α_{wet}	wet soil albedo (-)
β	coefficient describing rate of hydraulic conductivity increase with water content (-)
Λ	leaf area index (-)
Λ_{max}	maximum achievable LAI (-)
Λ_{ref}	reference LAI determining canopy cover (-)

1. MODEL OVERVIEW

1.1 Processes described

The Australian Water Resources Assessment system Landscape model (AWRA-L) is a grid-distributed biophysical model that simulates water stores and flows in the vegetation, soil and local catchment groundwater systems. The model aims to produce interpretable water balance component estimates, and as much as possible agree with water balance observations, including point gauging data and satellite observations. The model is intended to be parsimonious rather than comprehensive, to supports its use at moderate (1-10 km) resolution and in environments with few on-ground observations to constrain it. However in some instances a compromise needed to be found between a desire for parsimony and the requirement to simulate particular water balance terms.

The present version of AWRA-L uses relatively simple, lumped models of catchment water balance and vegetation ecohydrology and phenology[1]. The model currently includes descriptions of the following stores, fluxes and processes (equations and their justification are described further on):

- partitioning of precipitation between interception evaporation and net precipitation;
- partitioning of net precipitation between infiltration, infiltration excess surface runoff, and saturation excess runoff;
- surface topsoil water balance, including infiltration, drainage and soil water evaporation;
- shallow soil water balance, including incoming and exiting soil drainage and root water uptake;
- deep soil water balance – same as above;
- groundwater dynamics, including recharge, capillary rise and discharge; and
- surface water body dynamics, including inflows from runoff and discharge, open water evaporation and catchment water yield.

In addition, the following vegetation processes are described:

- transpiration, as a function of maximum root water uptake and optimum transpiration rate; and
- vegetation cover adjustment, in response to the difference between a actual and a theoretical optimum transpiration, and at a rate corresponding to vegetation cover type.

The processes represented by the model are illustrated in Figure 1. Many of the equations used are either the simplest formulation that can be expected to lead to reasonable results; have been directly derived from observations; or were selected through comparison against observations. As much as possible, the design of AWRA-L is modular to allow alternative process

[1] *phenology*: relating to cyclical biological events in response to climatic conditions, in particular greening and senescence in response to water availability.

descriptions to be implemented. Formal inter-comparison experiments are underway and will lead to future improvements.

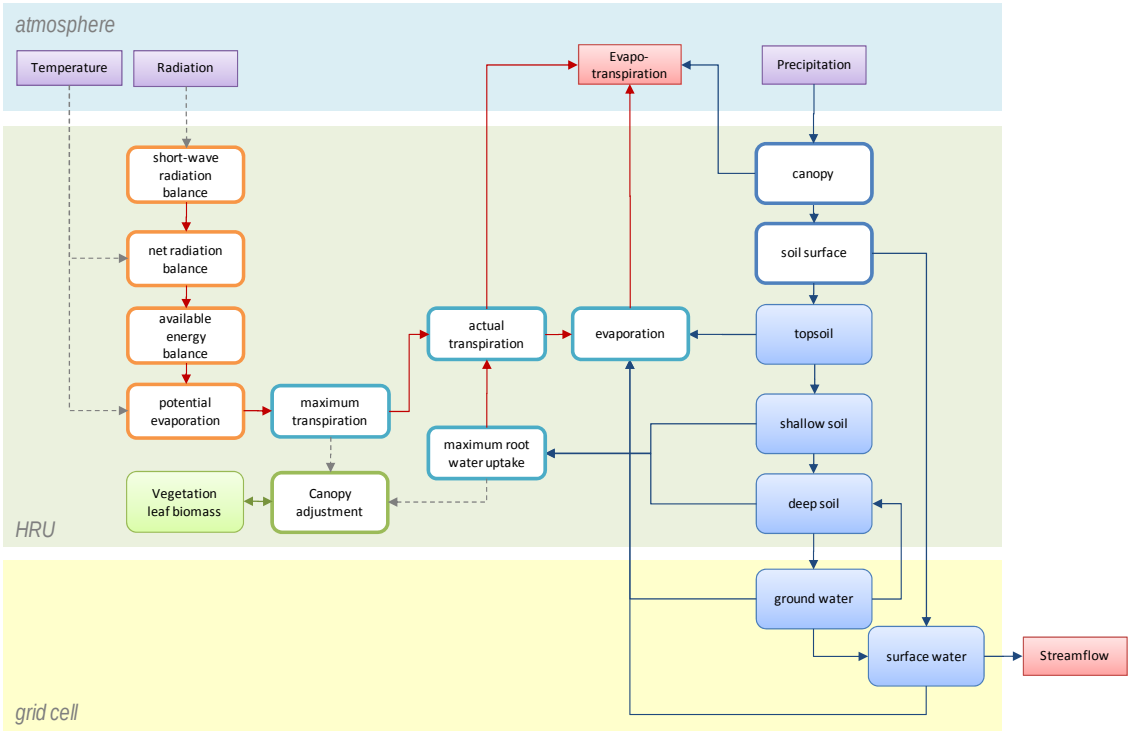

Figure 1. Simplified conceptual diagram of the AWRA-L model structure. Shown are: the minimum dynamic model inputs (purple); aggregated water losses from the grid cell (red boxes); water fluxes (blue arrows); energy and vapour fluxes (red arrows), and some key functional relationships (dashed grey arrows); water balance model components described in Section 2 (blue rounded boxes); the surface radiation and energy balance (orange, Section 3); vapour fluxes (cyan, Section 4); and vegetation phenology (green, Section 5). Solid blue and green colours represent dynamic model states persisting from one time step to the next; outlined boxes represent transformations and partitioning.

1.2 Spatial representation

Representation of lateral water exchanges

AWRA-L is a one-dimensional, grid-based water balance model that has a lumped representation of the water balance of the soil, groundwater and surface water stores. The elementary volume considered by the model is that of a small catchment (a 'representative elementary watershed'; Reggiani *et al.* 1998). It is assumed that such a model can be applied to grid cells of a representative size without introducing errors, or at least those errors disappear when aggregating to larger scales (the current application is at 0.05° covering all of Australia). For practical reasons, the current model version makes a very important assumption in that ***lateral redistribution between grid cells can be ignored without degrading water balance estimates***.

This leads to the following corollary assumptions:

(1) precipitation within the grid cell is the only source of water.

(2) groundwater systems are smaller than the model grid cell and therefore discharge within the grid cell; and

(3) hillslope hydrological processes (redistribution of surface, soil and groundwater at hillslope scale) are implicit in some of the model equations but not explicitly described.

The first assumption is obviously violated for large surface water bodies; in floodplains that are replenished by surface water; and in areas where groundwater is extracted from aquifers that are recharged by surface water or receive important groundwater influxes from adjoining areas. The estimated distribution of inflow dependent ecosystems (IDEs), that is, regions where ET is increased due to lateral inflows, is illustrated in Figure 2.

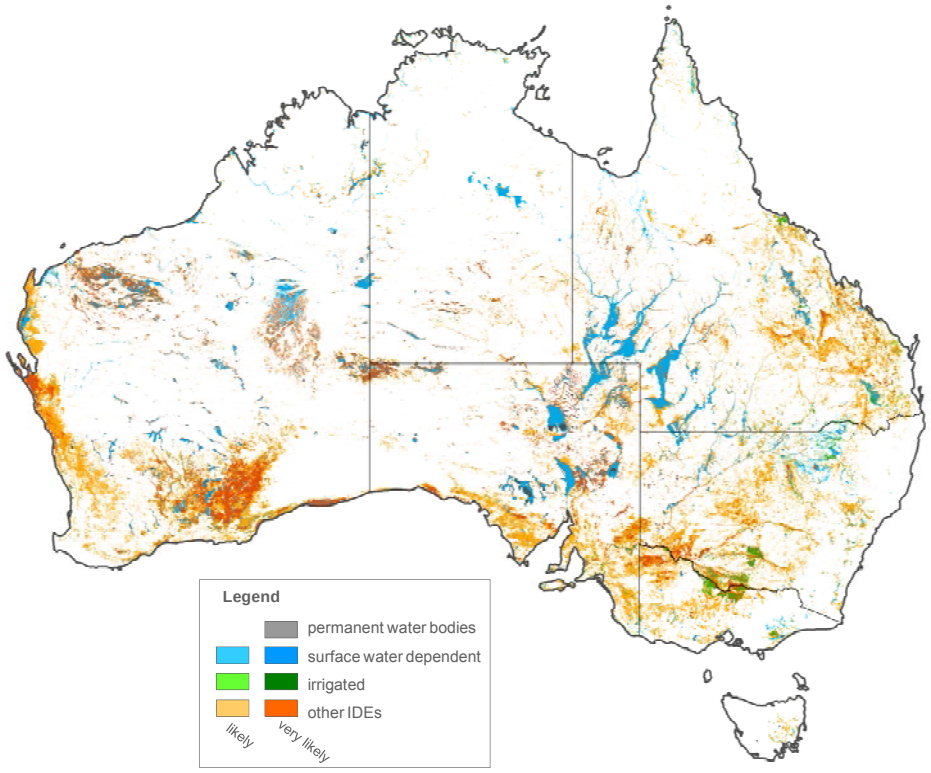

Figure 2. Estimated distribution of lateral flow receiving areas, or 'inflow dependent ecosystems'; IDEs, at 500m resolution (Van Dijk *et al.* 2010a). The likelihood of IDE occurrence was estimated by comparing dry land reference ET estimated by AWRA-L version 0.5 and bias-corrected actual ET estimated from MODIS satellite observations (Guerschman *et al.* 2009) for the period 2000-2009. The nature of inflows was attributed using ancillary information on inundation (also from MODIS; Guerschman *et al.*, in prep.) and land use (from the ACLUMM project). Note that mapping of 'other IDEs' (including groundwater inflow dependent ecosystems) could also reflect use of precipitation stored before the analysis period (that is, soil moisture or groundwater 'mining') or reflect errors in the method or its inputs.

The assumption of negligible lateral flow is increasingly likely to be violated as the grid resolution is increased. At 25 km resolution lateral soil and groundwater flows across unit boundaries are likely to be sufficiently small for their effect on the soil water balance and streamflow generation to be ignored, although surface water inputs (inundation, irrigation) may still be significant at this scale. At 1 km resolution lateral groundwater inflows may represent an important source of water (for example in highly conductive, well-connected alluvial aquifers). At 50 m resolution – smaller than the drainage spacing and average length of hill slopes in many areas – lateral redistribution of flows over the surface by run off–run on processes and through the unsaturated soil can become important.

AWRA-L is designed for observation-driven modelling. Since observations relevant to hill slope processes are generally lacking, explicit description of these 'sub-grid' processes is not attempted. Lateral surface and groundwater flows over larger distances (through rivers, man-made infrastructure and regional groundwater systems) are not described in AWRA-L, but are obtained by coupling AWRA-L to separate river and aquifer models within the AWRA system (See 'AWRA Technical Report 1: System Design'). This enables explicit accounting for the water balance of rivers and water bodies themselves, estimating lateral inflows of surface and groundwater to the surface and root zone, estimate extractions of surface water for consumptive

use, and replacing the grid-based groundwater description with a different (e.g. regional) groundwater model where appropriate. Improving the representation of regional groundwater systems and lateral flow exchanges between rivers, connected groundwater systems and the landscape are a current development focus. It is anticipated that independent estimates of ET based on satellite observations will be assimilated in future to estimate and account for lateral inflows within future versions of AWRA-L. At present, the influence of the 'no lateral flow' assumption needs to be carefully considered as a caveat when interpreting or using model estimates.

Hydrological response units

The landscape hydrological model has a grid-based structure. Each grid cell can contain one or more hydrological response units (HRUs). Soil and vegetation water and energy fluxes are simulated separately for each of HRU, and each HRU within each grid cell can be assigned different parameters representing soil and vegetation properties. Groundwater and river water dynamics are simulated at grid cell level and hence parameters are equal across the grid cell and dynamic variables (e.g. fraction groundwater saturated area and open water within stream channels) equal between HRUs.

The model structure has been designed to be flexible, allowing any number of one HRUs to be used, e.g. to represent alternative land use, cover or management regime. For operational applications it may need to be considered that in the extreme case increasing the number of HRUs changes may increase computational load proportionally, depending on other processes in the system workflow.

The present implementation of AWRA-L distinguishes two HRUs: tall, deep-rooted vegetation and short, shallow-rooted vegetation (Figure 3). This was considered justified by the different rooting and water uptake behaviour associated with these respective vegetation types. The recommended parameter values of the respective vegetation types are such that deep-rooted vegetation continues to have access to soil water during dry periods and has a canopy that fluctuates less rapidly in response to water availability. As a consequence, it has a canopy that fluctuate less over time than does the canopy of shallow-rooted vegetation. The consideration of only two land cover types is an obvious simplification; in reality there are vegetation types that combine characteristics of the two HRUs (e.g. drought-deciduous trees, deep-rooted short vegetation, etc), transient vegetation types, and areas that have no vegetation altogether. Since all model parameter can be provided as constants or as continental surfaces, regional differences in vegetation properties for the two main classes are readily described where available.

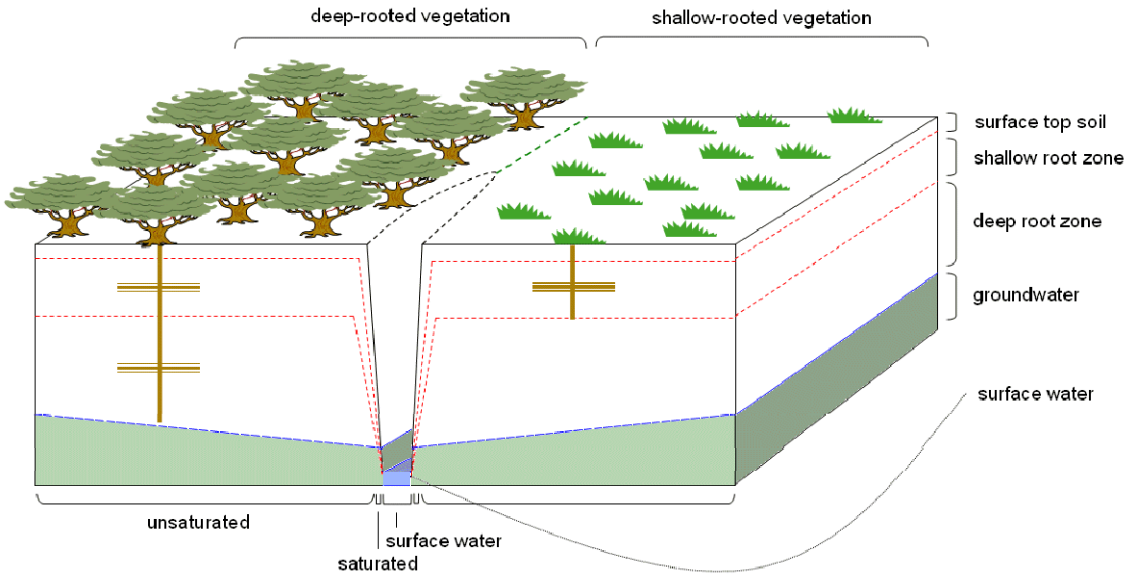

Figure 3. Diagram representation of the spatial components represented within a grid cell in the AWRA-L model. On the right the water stores considered by the model (blue dashed line indicates water table, red dashed lines boundaries between soil layers); at the top the hydrological response units (HRUs); and at the bottom the dynamic hydro-morphological landscape components.

1.3 Guide for reading

In the remainder of this report, all model equations are listed and discussed. The processes simulated are organised into four sections, pertaining to the movement of liquid water (Section 2), the surface energy balance and potential ET (Section 3), the evaporative or vapour fluxes (Section 4), and the algorithms used to describe vegetation phenology (Section 5). In each of these sections, the mass, radiation and energy balance equations are provided first, followed by any conversion equations used to translate between units. The remainder of each of the sections lists all equations to estimate the individual terms of the balance equations. Each equation is listed along with the variables and parameters that are associated with it, followed by a rationale explaining why the equation was chosen in favour of any alternatives or how it was developed, and a brief discussion on the likely range of values for any parameters in the equation that need to be estimated. In Appendix B the code of the MATLAB™ version of the AWRA-L version 0.5 time step model is listed.

2. WATER BALANCE

2.1 Mass balance equations

The water stores and fluxes described in AWRA-L are illustrated in Figure 4.

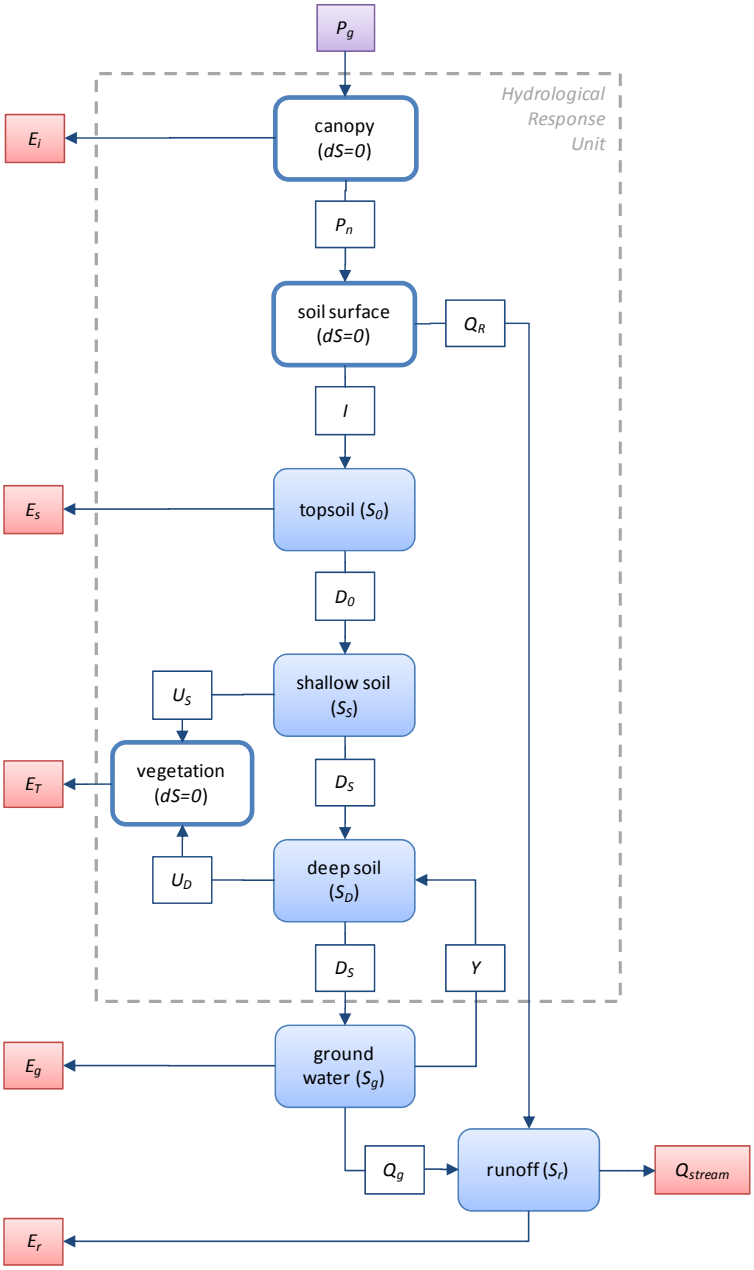

Figure 4. Flow diagram illustrating the water balance components for a Hydrological Response Unit (HRU). Shown are the internal stores (blue boxes), internal fluxes (outlined boxes), precipitation input (purple), and losses (red).

The mass balance equations used to describe the water balance are as follows:

Canopy partitioning of precipitation (P_g) into net precipitation (P_n) and interception evaporation (E_i) (no storage term):

$$P_n(t) = P_g(t) - E_i(t) \quad [2\text{-}1]$$

Soil surface partitioning of P_n into surface runoff (Q_R) and infiltration (I) (no storage term):

$$I(t) = P_n(t) - Q_R(t) \quad [2\text{-}2]$$

Surface top soil water balance, comprising top soil water storage (S_0), infiltration, soil evaporation (E_S) and top soil drainage (D_0):

$$S_0(t+1) = S_0(t) + I(t) - E_s(t) - D_0(t) \quad [2\text{-}3]$$

Shallow soil water balance, comprising shallow soil water storage (S_S), shallow root water uptake (U_S), top soil drainage (D_0) from the layer above, and shallow soil water drainage (D_S):

$$S_s(t+1) = S_s(t) + D_0(t) - U_S(t) - D_S(t) \quad [2\text{-}4]$$

Deep soil water balance, comprising deep soil water storage (S_D), D_S, capillary rise from the groundwater (Y), deep root water uptake (U_D), and deep drainage (D_D):

$$S_D(t+1) = S_D(t) + D_S(t) + Y(t) - U_D(t) - D_D(t) \quad [2\text{-}5]$$

Groundwater balance, comprising ground water storage (S_g), D_D, Y, groundwater evaporation (E_g) and groundwater discharge (Q_g):

$$S_g(t+1) = S_g(t) + D_D(t) - E_g(t) - Q_g(t) - Y(t) \quad [2\text{-}6]$$

River water balance, comprising surface water storage (S_r), Q_R, Q_g, and stream discharge (Q_{stream}):

$$S_r(t+1) = S_r(t) + Q_R(t) + Q_g(t) - E_r(t) - Q_{stream}(t) \quad [2\text{-}7]$$

In theory, some of the above mass balance could lead to negative storage values. In practice, this is prevented by order and structure of calculations of the respective fluxes (see model code in Appendix B).

The remainder of this section describes the equations used to estimate the various liquid water fluxes, but not the equations to estimate the evaporative loss terms (E_i, E_r, E_s and E_g); these are described in Section 4.

2.2 Conversion equations

Several of the equations use relative water content of the respective layers as a variable. It is defined here as:

$$w_z = \frac{S_z}{S_{zFC}} \qquad [2\text{-}8]$$

where S_z (mm) is the amount of water stored in layer z, and S_{zFC} (mm) the available water content at field capacity. It is assumed equal to the difference between water remaining in layer z one day after a saturation event (in line with the commonly used definition of field capacity) and the remaining soil water remaining when evaporation (in the case of S_0) or root water uptake (in the case of S_S and S_D) cease. This definition is chosen to avoid unnecessary parameters (see Ladson *et al.* 2004; Van Dijk and Marvanek 2010). The terms 'plant available water' and 'extractable water' have been suggested to describe the definition used here (Ladson *et al.* 2004).

2.3 Surface runoff (Q_R)

Equations

$$Q_R = \left((1 - f_{sat}) \frac{P_n}{P_n + P_{ref}} + f_{sat} \right) (P_n - I_i) \quad [2\text{-}9]$$

with

$$I_i = \min(P_n, I_0) \quad [2\text{-}10]$$

$$f_{sat} = \min\left(1, \max\left(\frac{S_G}{S_{Gref}}, f_{water}\right)\right) \quad [2\text{-}11]$$

Variables

Q_R estimated event surface runoff (mm)

f_{sat} groundwater saturated area fraction (-)

f_{water} fraction area covered by water (-)

P_n net event precipitation (mm)

P_g gross event precipitation (mm)

E_i interception evaporation (mm) (see Section 4.2)

I_i initial infiltration (mm)

Parameters

I_0 initial retention capacity (mm)

P_{ref} reference storm size (mm)

S_{Gref} reference groundwater storage (mm)

Rationale

The equations used were selected after comparing the explanatory value of alternative approaches used in existing models. They were tested against streamflow data from 260 Australian catchments, separated into storm flow and baseflow components (Van Dijk 2010).

The two terms between brackets in Eq. [2-8] can be interpreted to describe infiltration excess and saturation overland flow, respectively, although there is currently no direct evidence to support or reject this interpretation. The initial infiltration I_i represents the infiltration of water to wet the soil before any surface runoff occurs.

Application of this model using daily precipitation accumulations introduces the assumption that these daily accumulations represent a single individual storm event for each day. Rainfall intensity is known to have strong influence on infiltration-excess surface runoff generation.

They are implicit in the formulation through the correlation between daily rainfall and intensity statistics (Van Dijk 2010). If spatial data on intra-storm rainfall intensity become available, the process description can be improved in future versions.

Parameter estimation

P_{ref} can be interpreted as the hypothetical precipitation event size for which half of net precipitation on unsaturated soils is able to infiltrate and the other half runs off (cf. Eq. [2-8]). The parameter can be assumed to be related to the distribution in soil infiltration capacity values but also precipitation intensity. Using streamflow data, P_{ref} values were inferred that varied several orders of magnitude (90% between 254 and 10^6 mm), approximately following a log-normal distribution with a median of 1343 mm (Van Dijk 2010).

The same analysis found that fitting the value of initial retention capacity (I_0) produced a median value of 8 mm (90% of values of zero to 41 mm). Calibrating rather than prescribing I_0 led to minimal improvement in model performance. Implicit in I_i values estimated by Van Dijk (2010) are the effects of precipitation retention on the canopy. In AWRA-L, however, canopy retention is accounted for separately in the current version and may be up to ca. 3 mm (see Section 4.2). Therefore a default estimate of I_0=5 mm (that is, 8 less 3 mm) is suggested.

S_{Gref} represents the hypothetical groundwater storage at which the entire catchment area is saturated, and is a grid cell parameter that needs to be estimated. Van Dijk (2010) found that values for S_{Gref} for the 260 catchments analysed were approximately log-normally distributed with most values between 14 and 846 mm. Catchment mean annual precipitation (MAP) could explain 28% of the variation in S_{Gref} among 260 catchments following:

$$S_{Gref} = 8.15 MAP^{2.34} \qquad [2\text{-}12]$$

It follows that saturated area increases faster with increasing groundwater storage for a catchment with lower precipitation than for a catchment with comparatively higher precipitation. Another 32% of the variance among catchment S_{Gref} values was spatially correlated over distances of ~200 km, suggesting a relationship with underlying terrain rather than additional climate factors, which were correlated over longer distances. That implies that a prior estimates of S_{Gref} can be improved by considering spatial correlation using statistical techniques (Van Dijk 2010).

2.4 Root water uptake (U)

Equation

$$U_S = \min\left[S_S, \left(\frac{U_{S\max}}{U_{S\max} + U_{D\max}} \right) U \right] \quad [2\text{-}13]$$

and

$$U_D = \min\left[S_D, \left(\frac{U_{D\max}}{U_{S\max} + U_{D\max}} \right) U \right] \quad [2\text{-}14]$$

Variables

S_D deep soil water storage (mm)

S_S shallow soil water storage (mm)

U total actual root water uptake (mm d^{-1})

U_D actual root water uptake from deep soil (mm d^{-1})

$U_{D\,max}$ maximum root water uptake from deep soil (mm d^{-1})

U_S actual root water uptake from shallow soil (mm d^{-1})

U_{Smax} maximum root water uptake from shallow soil (mm d^{-1})

Rationale

Total U equals total transpiration E_t (see Section 4.3). In line with plant hydraulic theory, this actual transpiration is assumed to originate preferentially from those roots that experience the lowest matrix potential difference with the surrounding soil, and is limited by the maximum root water uptake from each layer (see Section 4.4).

2.5 Soil water drainage (D_z)

Equation

For each soil layer Z (with subscript Z replaced by 0, S or D as appropriate):

$$D_Z = f_{drain} S_Z \qquad [2\text{-}15]$$

with

$$f_{drain} = \max\left(K_{FC}, 1 - \frac{1}{w_Z}\right) \quad \text{if } w_Z > 1 \qquad [2\text{-}16]$$

$$f_{drain} = K_{FC} \exp\left[-\beta\left(1 - w_Z\right)\right] \quad \text{if } w_Z \leq 1 \qquad [2\text{-}17]$$

Variables

D_z drainage from layer z (mm d^{-1})

S_z water storage in layer z (mm)

f_{drain} drainage fraction (-)

w_z relative water content of layer z (-)

Parameters

K_{FC} drainage fraction at field capacity (-)

β drainage function exponent (-).

Rationale

Coarse resolution (e.g. >10 km) land surface schemes used in climate models and fine resolution (e.g. <100 m) or essentially one-dimensional soil water balance models, both commonly use a multi-layered soil to resolve the vertical fluxes of water. These fluxes are generally estimated by combining Richard's equation with a set of equations describing the relationship between soil moisture content, matric potential, hydraulic conductivity, and from these, moisture flux (e.g. the Brooks-Corey or Van Genuchten models; Rawls *et al.* 1992). While this would theoretically seem the most accurate way to describe soil moisture fluxes at high spatial resolution for homogenous alluvial soils in low relief terrain, a varying number of the assumptions underlying this approach are violated at coarser spatial resolution and in non-alluvial landscapes. Importantly among these in the context of the AWRA system are: (1) the predominant influence of soil components other than the soil matrix in controlling moisture flux at high water content – including large, connected biogenic pores and solid objects such as stones and roots; and (2) the high lateral variability in soil properties that occurs at sub-grid scale. As a consequence, use of matrix-related soil hydraulic parameter values estimated from mapped soil properties (e.g. texture classes) using so-called pedotransfer functions (Bouma 1989) can produce poor model behaviour at large scales (in particular, insufficient drainage and excessive saturation). The assumptions underlying a Richards-type model are probably better

approximated at lower soil moisture content, after larger pores have drained in the initial phases of dry down and moisture flux is indeed controlled by matrix flow (that is, below field capacity). It was considered that this did not justify the considerable computational costs involved with implementing a multi-layer Richards scheme; the number of poorly constrained 'effective' soil hydraulic and soil geometric parameters that would be needed, and – given the strong non-linearity of process response - the errors introduced by use of such an approach at large scale with these 'effective' parameter values.

Instead, it was attempted to retain some of the functional behaviour of a Richards solution, while adopting a simpler approach overall. High vertical and temporal resolution numerical experiments were performed with a model that used Richards' equation parameterised with Brooks-Corey relationships. Based on the results, a much simpler equation was derived that could adequately describe the simulated soil moisture behaviour. The experiments and model development are described in AWRA background paper 2010/1 (Van Dijk and Marvanek 2010) and resulted in the equations used here. The performance of this drainage model was compared with that of simple 'bucket' (that is, linear reservoir) models commonly used in Explicit Soil Moisture Accounting (or ESMA-type; Beven 2004) lumped rainfall-runoff models, such as HBV, Sacramento and SIMHYD (Burnash *et al.* 1973; Bergström and Singh 1995; Lindström *et al.* 1997; Chiew *et al.* 2002). The simplified Richards approach was shown to perform slightly better in explaining drainage estimated through hydrograph analysis for 198 catchments. More importantly, the parameters appeared better constrained and could actually be related back to the Brooks-Corey parameters used in the underlying multi-layer model (Van Dijk and Marvanek 2010).

Parameter estimation

Van Dijk and Marvanek (2010) calibrated model parameters K_{FC}, β and S_{FC} by fitting the model structure against drainage estimates derived by decomposition of streamflow observations of 198 Australian catchments into groundwater recharge pulses. However in that analysis, a single free draining soil layer was used, rather than the three soil layers conceptualised in AWRA-L. This is not expected to affect the relevance of K_{FC} and β values.

Values found for total available water storage at field capacity for a one-layer model had a median of 371 mm (mean 566 mm), and 50% of values were between 266–588 mm. 24% of the variance between catchments was correlated to the average annual minimum value of satellite observed vegetation greenness (MODIS EVI); interpreted as an indicator of the fractional cover of evergreen, deeper-rooted vegetation. The regression equation suggest a total storage of ca. 138 mm for catchments with very little tree cover, and values up to around 1000 mm in forested catchments. These values seem reasonable when compared to expected 'plant available water capacity' provided by the ASRIS[2] data base and rooting depths that can be expected for the two vegetation types.

Prior estimates of the parameters K_{FC} and β can in principle also be obtained using existing pedotransfer functions to estimate Brooks-Corey soil hydraulic parameters (Van Dijk and Marvanek 2010). The values for the parameter β derived by model fitting agreed extremely well with the prior estimates of 0.7 to 8.4 (median 4.5). Testing showed that this parameter could be prescribed at the median value 4.5 without degrading model performance and this is a recommended default parameter value. The K_{FC} values fitted were also in accordance with Brooks-Corey theory, with about half of the values falling within the range of 0.01 to 0.06 expected *a priori*. The median fitted value was 0.029 (mean 0.083). A relationship was found with climate wetness ($H=P/E_0$) of the catchments, explaining 40% of the variance:

[2] Australian Soil Resource Information System (*http://www.asris.csiro.au/*)

$$K_{FC} = 0.0685H^{3.18} \quad (r^2=0.40,\ N=198) \qquad [2\text{-}18]$$

This suggests that soils in comparatively wetter catchments are better drained. This is consistent with published differences in soil drainage and infiltration capacity – everything else being equal – between humid zone and arid zone soils. This contrast is most likely explained by the influence of vegetation and other biological processes on infiltration capacity (Jones *et al.* 1997; Dunkerley 2002).

2.6 Groundwater discharge (Q_g)

Equation

$$Q_g = \left[1 - \exp\left(-K_g\right)\right] S_g \qquad [2\text{-}19]$$

Variables

Q_g groundwater discharge into stream (mm d^{-1})

S_g groundwater reservoir storage (mm)

Parameters

K_g groundwater drainage coefficient (d^{-1}).

Rationale

The one-parameter formulation chosen here is known as a linear reservoir equation and is commonly used in lumped catchment rainfall-runoff models (Jakeman and Hornberger 1993; Beven 2004). The most commonly used alternative is the two-parameter non-linear reservoir equation, where S_g is raised by an exponent, as for example in the PDM model (Moore 2007). Using daily streamflow data for 183 Australian catchments, both linear and non-linear equations were evaluated (Van Dijk 2009). It was concluded that there was insufficient basis in the observations to prefer a two parameter (non-linear) reservoir model over a single parameter (linear) model. As any analysis based on streamflow observations, it needed to be assumed that groundwater drainage is broadly equivalent to 'baseflow' and therefore that K_g is equivalent to the baseflow or recession coefficient. This is consistent with common rainfall-runoff model structures, however the assumption itself is not necessarily valid. Firstly, 'baseflow' can include contributions from slowly releasing stores other than groundwater, such as very slow draining soils, perched groundwater tables or wetlands. Depending on how the groundwater reservoir is defined these contributions may or may not be included in the model used here. Secondly, discharged groundwater may evaporate from the surface before reaching the river or from the river before reaching a downstream point of reference. Indeed, at very low streamflow rates faster recessions have been observed than predicted by the linear equation (Van Dijk 2009). This may well be due to the observable influence of evaporation losses at low flow rates, which were not estimated in the streamflow analysis. Evaporation from groundwater saturated areas (E_g) and direct evaporation from the river (E_r) are accounted for in AWRA-L, however (see Section 4).

Parameter estimation

For the 183 Australian catchments investigated as part of model development (Van Dijk 2009) an average K_g value of 0.060 was found (st.dev. ±0.029). Values appeared approximately log-normally distributed, and 80% of values were in the range 0.030–0.095. The authors found some correlation between K_g and climate wetness (H), implying that a catchment in a comparatively wetter climate will on average show slower baseflow recession than one in a drier climate. A best fit power relationship was calculated as:

$$K_g = 0.0470H^{-0.0508} \qquad (r^2=0.27,\ N=183) \qquad [2\text{-}20]$$

Semi-variogram analysis showed that much of the residual variance (53% of total variance) was spatially correlated over length scales of up to 200 km, which was attributed to catchment geomorphology. This implies that spatial interpolation techniques can help improve prior K_g estimates if streamflow observations are available within a few hundred kilometres.

2.7 Capillary rise (Y)

Equation

$$Y = F_{DG}\left(w_{\lim D} - w_D\right)S_g \qquad \text{if } w_D < w_{limD} \qquad [2\text{-}21]$$

$$Y = 0 \qquad \text{if } w_D \geq w_{limD} \qquad [2\text{-}22]$$

Variables

Y capillary rise of groundwater into deeper root zone (mm)

w_D relative deep root zone water content (–)

S_g groundwater reservoir storage (mm)

Parameters

w_{limD} deep root zone water content at which root water uptake is limited (-)

F_{DG} connectivity between soil and groundwater (-)

Rationale

The main purpose of this equation is to allow some degree of upward moisture flux between groundwater and the deep root zone as would result from root water uptake in the capillary zone. In the absence of influx from the overlying soil layer, and in the presence of a groundwater table sufficiently nearby, water extraction in the root zone will disrupts the equilibrium soil moisture profile, causing groundwater to move into the unsaturated zone to restore equilibrium.

Capillary rise may be important to sustain transpiration from deep-rooted, evergreen vegetation through the dry season. For example, flux tower ET measurements in Northern Australia (Howard Spings, NT and Virginia Park, Qld) suggest that the tree component in the savannah can steadily maintain dry season transpiration rates on the order of 0.5-1.0 mm d^{-1} (see data in AWRA Technical Report 4). It is unknown is to what extent this water use depletes the deep root zone and to what extent the removed water is replaced by capillary rise; uptake from the saturated zone itself would seem less likely due to the prolonged saturated conditions the roots would need to be adapted to.

The relationship between capillary rise and deep root zone water content will depend on the vertical pattern (depth) of water uptake, the distance to the groundwater table, and the soil water - hydraulic conductivity relationship for the unsaturated zone between roots and groundwater table.

These properties are poorly known, and therefore a very simple description was chosen that allows the two extreme and intermediate situations to be simulated. A simplifying assumption is made here that capillary rise occurs when relative water content in the deep root zone becomes limiting for root water uptake (w_{limD}). If F_{DG} is unity than the deep root zone and groundwater are strongly connected and effectively water uptake from the deep root zone is immediately replaced by groundwater. If F_{DG} is zero, there is no connectivity and the deep root zone is only

replenished by drainage from the shallow root zone. For intermediate values, capillary rise occurs but is insufficient to restore the equilibrium profile. Which F_{DG} value provides the better description would be expected to depend on the difference between the fluxes of root water uptake and capillary rise.

Since capillary rise is only estimated for the deeper soil layer, no capillary rise is simulated for the HRU with shallow-rooted vegetation, nor is any soil moisture simulated to rise from the shallow soil to the topsoil to sustain higher soil evaporation rates. These are simplifications that may lead to considerable errors where the groundwater table is close to the surface over large areas. If continental data on groundwater depth become available, the approach followed here should be considered for improvement.

Parameter estimation

The parameter F_{DG} interacts with the choice of maximum deep root water uptake rate (Section 4.4). As a default, it is assumed that the groundwater table is sufficiently close so that root water uptake from the deep soil layer can be replaced by capillary rise and therefore F_{DG} may be prescribed a value of unity.

2.8 Streamflow (Q_{stream})

Equation

$$Q_{stream} = [1 - \exp(-K_r)]S_r \quad [2\text{-}23]$$

Variables

Q_{stream} streamflow discharge from catchment (mm d^{-1})

S_r aggregrate depth of storage in freely draining surface water stores (mm)

Parameters

K_r streamflow drainage coefficient (d^{-1})

Rationale

Total streamflow discharge is estimated in a manner equivalent to that of groundwater drainage. The purpose of this store is primarily to reproduce the partially delayed drainage of storm flow that is normally observed in all but the smallest and fast-responding catchments. It also allows simulation of the transient storage of surface water in the landscape and the associated open water evaporation (Section 4.7). Because K_r is in the order of magnitude of the modelling time step and precipitation input information (one day), the agreement between the timing of the peak in observed storm flow response and those simulated by the model is often rather poor. This may be exacerbated by the difference in aggregating period (ending 9 am for precipitation, but normally at midnight for streamflow). Therefore good agreement between the timing of runoff peaks should not necessarily be expected.

Parameter estimation

In a storm flow[3] analysis for 260 Australian catchments, the distribution of storm flow recession coefficients (equivalent with K_r) appeared normally distributed, with an average value of 0.77 and 80% of all values between 0.5–1.1 (Van Dijk 2010). It follows that storm flow half time was generally about a day. Travel times of ca. 0.1 day would be expected for channel flow for most catchments based on their size (29–1902 km^2, median 333 km^2). Therefore storm flow recession may have been more dominated by release of temporary retained or retarded water (e.g. ephemeral water bodies, draining soil, perched groundwater) and less by the travel time of overland and channel flow. This introduces some uncertainty in the conceptual definition of the store that is involved in storm flow routing.

Correlation analysis with catchment climate, terrain and land cover attributes suggested that catchment potential ET (E_0) could explain 23% of the variance in K_r. The most rapid drainage occurred in catchments with high E_0 (corresponding with dry conditions). The following relationship was derived:

[3] Storm flow was calculated in the analysis as the difference between total streamflow and baseflow estimated with a recursive filter (see Van Dijk, 2010)

$$K_r = 0.141E_0 + 0.284 \qquad (N=260,\ r^2=0.23) \qquad [2\text{-}24]$$

This relationship is statistical only, but is consistent with the expectation that storm flow in dry catchments would be predominantly through infiltration excess overland flow and therefore travel times fast. Another 41% of the variance appeared spatially correlated over length scales of up to 300 km, suggesting a combination of unresolved terrain and climate factors may be responsible. This means that data from nearby catchments can be used to reduce the uncertainty in K_r estimates.

It is noted that in the model groundwater discharge (baseflow) is also routed through this store before being converted into streamflow. As a result the associated groundwater discharge recession is not exactly equivalent to the baseflow recession observed in streamflow; nor is streamflow recession exactly equal to storm flow recession. The numerical difference will normally be negligible, because K_g and K_r will vary an order of magnitude or more, and because the delayed drainage of one days' baseflow is compensated by the delayed drainage from the day before.

3. RADIATION AND ENERGY BALANCE

3.1 Radiation and energy balance equations

The structure of the model component that estimates potential evaporation[4] from atmospheric variables and land surface characteristics is illustrated in Figure 5.

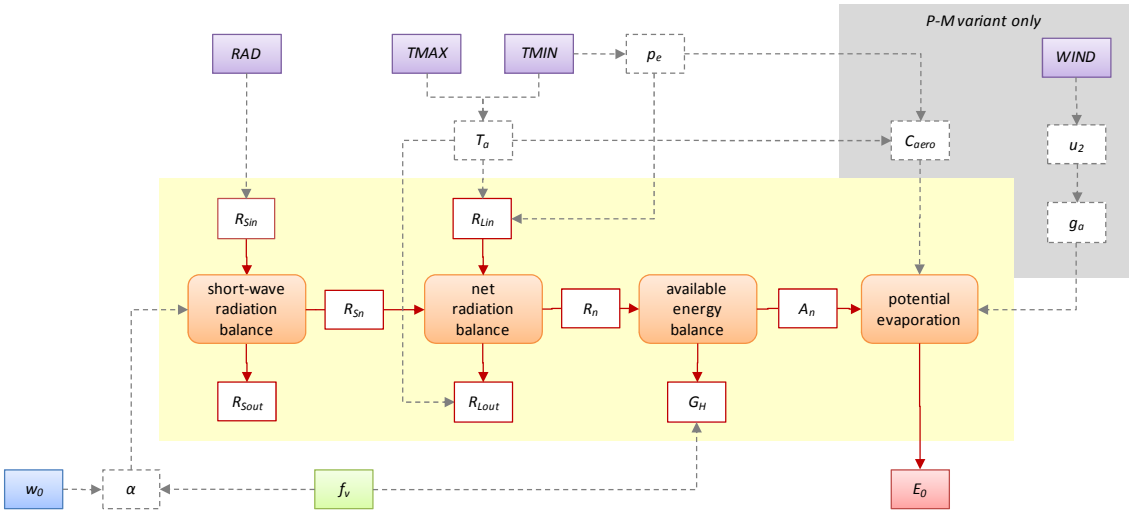

Figure 5. Flow diagram illustrating the energy balance calculations for a Hydrological Response Unit. Shown are the atmospheric drivers (purple), the linkages to vegetation and soil water variables (green and blue box, respectively), and the main output from the calculations (in red). Energy balance equations and energy fluxes are shown as orange shaded and outlined boxes respectively. The yellow background indicates the part of the model that performs energy calculations in W m^{-2}, whereas the grey shaded background shows a part of the model only used when the Penman-Monteith equation is applied.

The net radiation energy (R_n) received is the sum of net shortwave radiation (R_{Sn}) and net longwave radiation (R_{Ln}) inputs. These in turn are calculated from the incoming and outgoing shortwave radiation (R_{Sin} and R_{Sout}) and incoming and outgoing longwave (thermal) radiation (R_{Lin} and R_{Lout}) as:

$$R_n = R_{Sn} + R_{Ln} = R_{Sin} - R_{Sout} + R_{Lin} - R_{Lout} \qquad [3\text{-}1]$$

Note that all quantities are effective fluxes, that is, average fluxes during daytime (in W m^{-2}). During daytime conditions, a fraction of this energy input goes to soil heat flux (G_H) and hence is not available for evaporation.

$$A_n = R_n - G_H \qquad [3\text{-}2]$$

where A_n is the available energy that is converted to sensible and latent (ET) heat fluxes.

[4] The words 'evaporation' and 'evapotranspiration' and the acronym ET are used interchangeably here if they refer to the sum of (actual or potential) evaporation and transpiration fluxes.

Additional small additional amounts of energy may be used for photosynthesis or stored in biomass, and evaporation may occur at night-time. These fluxes are considered to be sufficiently small to ignore when compared to other sources of uncertainty (but see discussion in Section 3.7).

The two probably most common methods used to estimate ET in hydrological models are through use of the Penman-Monteith (P-M) combination equation (Monteith 1965), and the Priestley-Taylor (P-T) equilibrium evaporation equation (Priestley and Taylor 1972). An important difference between the two equations is that the P-M equation explicitly accounts for the effect of wind speed but requires wind speed data to do so; whereas the P-T approach makes simplifying assumptions that avoid the need for wind speed data. AWRA-L was designed to accommodate either approach by expressing both approaches in terms of a potential evaporative fraction (f_{E0}) to estimate potential evaporation (E_0 in mm d^{-1}; see Appendix A for details):

$$E_0 = f_{day} c_{RE} f_{E0} A_n \qquad [3\text{-}3]$$

where f_{day} is the fraction of daytime hours in a day and c_{RE} a unit conversion, which together convert from W m^{-2} to mm d^{-1}.

3.2 Conversion equations

Several empirical conversion equations are required to convert between radiation, conductance, energy and evaporation rate. These are based on well-established theory and estimation methods and provided in this section (see Appendix A.3 for derivation). The unit conversion coefficient c_{RE} between latent heat flux (W m^{-2}) and evaporation (mm d^{-1}) is given by:

$$c_{RE} = 0.03449 + 4.27 \cdot 10^{-5} T_a \qquad [3\text{-}4]$$

Where T_a (ºC) is effective air temperature.

The unit conversion C_{aero} from aerodynamic conductance (in m s^{-1}) to energy (in W m^{-2}) is required to estimate the aerodynamic component of PET in the P-M approach (cf. Section 3.8):

$$C_{aero} = 0.176\left(1 + \frac{T_a}{209.1}\right)\left(p_{air} - 0.417\, p_e\right)\left(1 - f_{RH}\right) \qquad [3\text{-}5]$$

with

$$p_{es} = 610.8 \exp\left(\frac{17.27 T_a}{237.3 + T_a}\right) \qquad [3\text{-}6]$$

$$f_{RH} = \frac{p_e}{p_{es}} \qquad [3\text{-}7]$$

where p_{air}, p_e and p_{es} are air and actual and saturated vapour pressure, respectively (Pa), and f_{RH} is relative humidity.

The dimensionless coefficient k_ε is used to estimate maximum evaporation. It is the ratio of the psychometric 'constant' over the slope of the function $p_{es}(T_a)$ relationship at ambient temperature (in the literature generally symbolised by ε or γ/Δ, respectively; cf. Appendix A.3):

$$k_\varepsilon = 1.40 \cdot 10^{-3}\left[\left(\frac{T_a}{187}\right)^2 + \frac{T_a}{107} + 1\right]\left(6.36\frac{p_{air}}{p_{es}} + f_{RH}\right) \qquad [3\text{-}8]$$

3.3 Estimation of effective values for meteorological variables

Energy balance equations are designed for use with instantaneous radiation fluxes and atmospheric properties, and therefore where they are combined with daily averages or totals, 'effective' atmospheric variables need to be estimated. Two meteorological products with Australia-wide coverage currently exist. Both provide gridded 0.05° resolution data sets: the SILO product[5] produced by the Department of Environment and Resource Management (Jeffrey *et al.* 2001) and the BAWAP product[6] produced by the Bureau of Meteorology (Jones *et al.* 2007; Jones *et al.* 2009). Both SILO and BAWAP data provide only one or two descriptors of the daily cycle in these variables, and therefore estimation equations are required to derive 'effective' values for meteorological variables for use in evaporation estimation.

Incoming shortwave radiation

Both SILO and BAWAP produce data on daily incoming shortwave radiation (RAD in MJ m^{-2} d^{-1}), which is converted *to* R_{Sin} (in W m^{-2} during daytime) as follows:

$$R_{Sin} = \frac{10^6}{186400 f_{day}} RAD = \frac{11.57}{f_{day}} RAD \qquad [3\text{-}9]$$

The annual average value f_{day}=0.5 is used in the current model version; the influence of this simplification on calculated E_0 is likely to be negligible. Astronomical equations to calculate the fraction daylight hours as a function of day of year and latitude do exist, however, and may be considered for future model versions.

Effective air temperature

Both SILO and BAWAP provide minimum and maximum diurnal temperature (*TMIN* and *TMAX* in °C; applicable to the 24 hours starting 9 am local time on the day of reporting). An effective average air temperature T_{a*} (ºC) is estimated as:

$$T_a = TMIN + 0.75(TMAX - TMIN) \qquad [3\text{-}10]$$

It is noted that several of the temperature-dependent functions used are strongly non-linear and therefore the above approximation will possibly introduce error, although its magnitude is unknown. Further work will be considered to develop more appropriate methods to correct for the errors introduced.

Effective vapour pressure

Both SILO and BAWAP provide data on vapour pressure at 9:00 am (*VP09* in hPa) whereas the BAWAP data set also provides data at 15:00 pm (*VP15*). Vapour pressure can also be estimated with useful accuracy using (e.g. McVicar and Jupp 1999):

$$p_e = p_{es}(TMIN) \qquad [3\text{-}11]$$

[5] www.longpaddock.qld.gov.au/silo
[6] www.bom.gov.au/jsp/awap

This effectively assumes that the air is near saturation when minimum temperature occurs (normally just before dawn). While this is not always the case, preliminary comparison with VP09 and VP15 data (unpublished) showed very reasonable agreement and hence this approach was used as a simplification, thus avoiding the need for VP09 data and reducing model run-time. It may be considered for refinement in future versions.

Effective air pressure

Measurements of air pressure at the land surface (p_{air}) are not readily available. The average air pressure at sea level is ca. 101500 Pa for Australia, and not often varies more than 2% from this value[7]. The average elevation of Australia is 330 m[8], from which an average air pressure at the surface of 97500 Pa can be estimated. This value was used. Improving air pressure estimates, while conceptually perhaps desirable, is likely to have negligible effect on water balance estimates due to the low sensitivity of estimated E_0 to air pressure. Refinements that could be considered for future model versions include use of a spatially varying long-term average p_{air} based on average pressure fields as well as surface elevation; or even the use of dynamic pressure fields from numerical weather prediction (NWP) models.

Effective wind speed

Daytime wind speed also typically has a diurnal course. Effective daytime wind speed (u_2 in m s^{-1}) is estimated from average daily wind speed as:

$$u_2 = \frac{\left[1-\left(1-f_{day}\right)0.25\right]}{f_{day}} WINDSPEED \qquad [3\text{-}12]$$

A continental daily average wind speed product was recently developed for 1975-2006 (McVicar *et al.* 2008) by interpolating daily averages of wind speed inside climate stations measured 2 m above the surface (WINDSPEED in m s^{-1}). On any given day, between 112 and 196 stations across Australia had data available that were used in interpolation. At present, the average continental daily wind speed of 2.0 m s^{-1} estimated by McVicar and colleagues was used. This leads to an estimated Australia-average *daytime* u_2 of 3.5 m s^{-1}; this value is suggested as a default.

Unlike air pressure, wind speed can potentially have considerable influence on calculated E_0 values, which in turn can affect actual ET estimates if ET is not only constrained by water availability. The potential for model performance improvements by using the McVicar *et al.* (2008) wind speed product or a derived spatial long-term average or climatology should be considered for future model versions. Wind fields from NWP models provide additional information that might be useful in improving ET estimates.

[7] Estimated from digital maps available from Bureau of Meteorology (http://www.bom.gov.au/jsp/ncc/climate_averages/mean-sealevel-pressure/index.jsp)
[8] Data from Geosciences Australia (http://www.ga.gov.au/education/geoscience-basics/landforms/elevations.jsp)

3.4 Daytime outgoing shortwave radiation ($R_{S,out}$)

Equation

$$R_{Sout} = \alpha R_{Sin} \quad [3\text{-}13]$$

with

$$\alpha = f_V \alpha_V + f_S \alpha_S \quad [3\text{-}14]$$

$$f_S = 1 - f_V \quad [3\text{-}15]$$

$$\alpha_S = \alpha_{wet} + (\alpha_{dry} - \alpha_{wet}) \exp\left(-\frac{w_0}{w_{\alpha,ref}}\right) \quad [3\text{-}16]$$

Variables

α shortwave albedo (-)

α_S soil surface albedo

f_V fraction vegetation canopy cover

f_S fraction soil cover

R_{Sin} incoming shortwave radiation (W m^{-2})

R_{Sout} outgoing shortwave radiation (W m^{-2})

w_0 relative soil moisture content of the top soil layer

Parameters

α_V vegetation canopy albedo

α_{wet} wet soil albedo

α_{dry} dry soil albedo

$w_{\alpha,ref}$ reference value of w_0 describing the relationship between albedo and top soil wetness

Rationale

The model adopted is about the simplest that can be conceptualised yet still allows changes in vegetation cover and soil wetness to be translated into albedo changes. Note that ‘soil’ is defined here as the faction of area not covered by vegetation canopy, which can be a combination of bare soil, dead biomass, rocks, and other materials.

Albedo varies as a function of the spectrum of the sunlight reaching the surface and atmospheric conditions. MODIS satellite albedo products are available for black sky (cloudless, direct radiation) and white sky (diffuse light conditions). Albedo values can range from 0.10 to wet dark soils, via ca. 0.13 for tall dark-leaved forests to more than 0.30 for fertilised agricultural crops and dry litter, respectively, and occasionally more than 0.50 for evaporites such as salt

lakes (Ross 1981; Shuttleworth 1992) Consequently, absorbed shortwave radiation, normally the main driver of evaporation, can vary from 50 to more than 90% of incident radiation.

The approach taken here is a simple linear mixing approach, whereby albedo is a fractional cover-weighted average of canopy and soil background albedo respectively. More elaborate radiation transfer models have been used (e.g. Ross 1981; Kowalczyk *et al.* 2006) to account for changing sun angle and multilayer canopy transfer effects. Due to limited availability of some key data (e.g. sub-daily irradiance, split between diffuse vs. direct radiation, canopy structure) their application would require important simplifying assumptions and uncertain parameters. This was considered incongruous with the overall modelling approach, that is, the complexity was not considered justified by the available observations or the model outputs required.

The equation describing the effect of soil moisture on surface albedo (Eq. [3-16]) is an empirical one based on a comparison of satellite derived albedo (MODIS) and relative top soil moisture (ASAR GM) measurements over Australia described in AWRA background paper 2010/2 (Van Dijk *et al.* 2010b).

Parameter estimation

The fractions of deep- and shallow-rooted canopy and soil surface moisture content are simulated by the model. The MODIS broadband white-sky albedo product was analysed by fitting a linear mixing model to derive values or empirical predictive equations to estimate albedo. The analysis is described in AWRA background paper 2010/2 (Van Dijk *et al.* 2010b). It produced α_V estimates of 0.166 for seasonally varying (assumed equivalent to shallow-rooted) vegetation cover and 0.135 for persistent (deep-rooted) vegetation, in line with values commonly found globally (e.g. Shuttleworth 1992). The photosynthetic capacity index (PCI, see Section 4.3) appeared to be a good predictor of canopy albedo using:

$$\alpha_V = 0.452 PCI \qquad [3\text{-}17]$$

Further analysis was done to analyse the effect of soil moisture. An average α_s of 0.22 was found, whereas average α_{dry} and α_{wet} were 0.26 and 0.16, respectively. Analysis of residuals showed that dry soil albedo varied across the continent, with 80% in the range 0.19–0.35. A value $w_{\alpha,ref}$ =0.30 produced the best fit to the observed relationship between soil wetness and albedo. At present, these spatially uniform average values of α_s, α_{dry}, α_{wet} and $w_{\alpha,\mathrm{ref}}$ are used. Refinements to the albedo may be considered for future model versions, in particular by including information on spatial variation in soil and canopy albedo (Van Dijk *et al.* 2010b). In addition, it could be investigated under what circumstances a climatology derived from the MODIS albedo product might provide better albedo estimates than model estimated albedo.

3.5 Daytime incoming longwave radiation ($R_{L,in}$)

Equation

$$R_{Lin} = f_{\varepsilon atm}\sigma(T_a + 273.16)^4 \quad [3\text{-}18]$$

with

$$f_{\varepsilon,atm} = 0.65\left(\frac{p_e}{T_a + 273.16}\right)^{0.14} \quad [3\text{-}19]$$

Variables

$f_{\varepsilon,atm}$ atmospheric emissivity (-)

σ Stefan-Bolzman constant ($5.6704 \cdot 10^{-8}$ W m^{-2} K^{-4})

p_e atmospheric vapour pressure (Pa)

$R_{L,in}$ incoming longwave radiation (W m^{-2})

T_a effective average air temperature (°C)

Rationale

The emission of radiation by a body is defined by the Stefan-Bolzman Law, whereas the emissivity of the atmosphere is estimated using the formulation proposed by Brutsaert (1975). The Brutsaert has recently been identified as the most accurate 'all-weather' method among several alternatives, including that of Prata (1996) (Sridhar and Elliott 2002; Duarte *et al.* 2006).

An underlying assumption is that R_{Lin} is sufficiently accurately estimated by considering daytime average air temperature and vapour pressure. Given the strong non-linearity of the relationship with temperature, this assumption may well introduce error. The assumption is necessary because of the lack of data on sub-daily air temperature and surface temperature, although a prescribed diurnal pattern (e.g. McVicar and Jupp 1999) or use of geostationary satellite observations could potentially reduce the associated error. An analysis of the sensitivity of E_0 to this assumption could be considered for future model versions.

3.6 Daytime outgoing longwave radiation ($R_{L,out}$)

Equation

$$R_{Lout} = f_{\varepsilon}\sigma\left(T_a + 273.16\right)^4 \qquad [3\text{-}20]$$

Variables

T_a effective average air temperature (°C)

R_{Lout} outgoing longwave radiation (W m^{-2})

σ Stefan-Bolzman constant ($5.6704 \cdot 10^{-8}$ W m^{-2} K^{-4})

Parameters

f_{ε} surface emissivity (-)

Rationale

Outgoing longwave radiation is defined by Stefan-Boltzmann's Law. As for incoming longwave radiation (Section 3.5), an underlying assumption is that R_{Lin} out is sufficiently accurate estimated by considering daytime average air temperature. The same caveats and possible avenues for future improvement therefore apply.

Parameter estimation

Emissivity (f_{ε}) is currently assumed equal to unity, which will be a slight overestimation of real emissivity (by 1–3%; Wan 2008). The effect of this on estimated E_0 values is further reduced due to other terms in the radiation and energy balance. Future improvements may include consideration of a mixing model that accounts for the difference in emissivity between vegetation canopy and the top soil for different moisture levels, e.g. based on analysis of the MODIS emissivity product (Wan 2008) or using an emissivity model developed for microwave radiation transfer modelling (e.g. Owe *et al.* 2001).

3.7 Ground heat flux (G_H)

Equation

$$G_H = F_{GR} R_n \quad [3\text{-}21]$$

with

$$F_{GR} = F_{GR,\max}\left[1 - \exp\left(-\frac{f_S}{F_{S,ref}}\right)\right] \quad [3\text{-}22]$$

Variables

F_{GR} fraction daytime net energy lost to soil heat flux (W m^{-2})

f_S fraction uncovered by vegetation canopy (-)

R_n net radiation (W m^{-2})

Parameters

F_{GRmax} fraction of daytime net radiation lost to soil heat storage for an unvegetated surface (-)

$F_{S,ref}$ reference soil cover fraction that determines the rate of decline in soil heat flux with increasing canopy cover (-)

Rationale

The model selected to estimate net surface heat flux is arguably one of the simplest possible, while still recognising that net surface heat flux will be greater for uncovered soil. The relationship is almost identical to the empirical equation proposed by Bastiaanssen *et al.* (1998), with NDVI replaced by fraction canopy cover, and the polynomial equation replaced by an extinction function of near-identical form (Figure 6). This extinction function was considered conceptually more preferable as is it in accordance with the Lambert-Beer relationship between vegetation leaf area and canopy cover (Section 5.3). It is assumed that G_H is the only non-negligible sink of daytime available energy besides sensible and latent heat fluxes. Some caveats are discussed below.

Firstly, the equation used here was developed for instantaneous day time fluxes, and therefore an assumption in its use is that release of heat from storage during the night does not to lead to evaporation. This corresponds with the assumption that ET ceases during the night, although in reality there can be night-time evaporation and even transpiration, particularly from well-watered ecosystems under dry, windy conditions. Field observations for an irrigated eucalypt plantation near Wagga Wagga, New South Wales, suggested that night-time ET could amount up to 5% of total ET on dry, windy nights (Benyon 1999), and even higher night-time ET rates (sometimes in excess of 20% of day-time ET) are reported by Dawson *et al.* (2007). Night-time ET is not necessarily in violation with the assumption that there is no heat release, as most of the evaporative energy is likely to be extracted from the air, causing cooling. However, inevitably it does lead to a systematic underestimation of ET during dry, windy conditions.

Secondly, the model does not account for differences in surface heat flux associated with soil moisture content. Soil moisture content affects heat capacity and conductivity and therefore this assumption will introduce some errors.

Thirdly, the model predicts that there is no heat storage (in the soil or elsewhere) at full canopy cover. This is probably an incorrect assumption for dense forests, where there may well be some heat storage in the vegetation biomass. In line with existing land surface models, it was assumed that the error introduced by these violations is insignificant compared to other sources of uncertainty. It is noted that full canopy cover will not actually be achieved in model simulations and therefore a small heat flux will always be simulated.

Parameter estimation

The collated field experimental data shown in Bastiaanssen *et al.* (1998) suggest $F_{loss,max}$ values of ca. 0.25 to 0.50; they adopted a best fit estimate of 0.30. Fitting Eq. [3-22] to those same data produced $F_{s,ref}$ values of around 0.2. A value of 0.22 was estimated by [3-22] to the polynomial model of Bastiaanssen *et al.* (1998) (Figure 6).

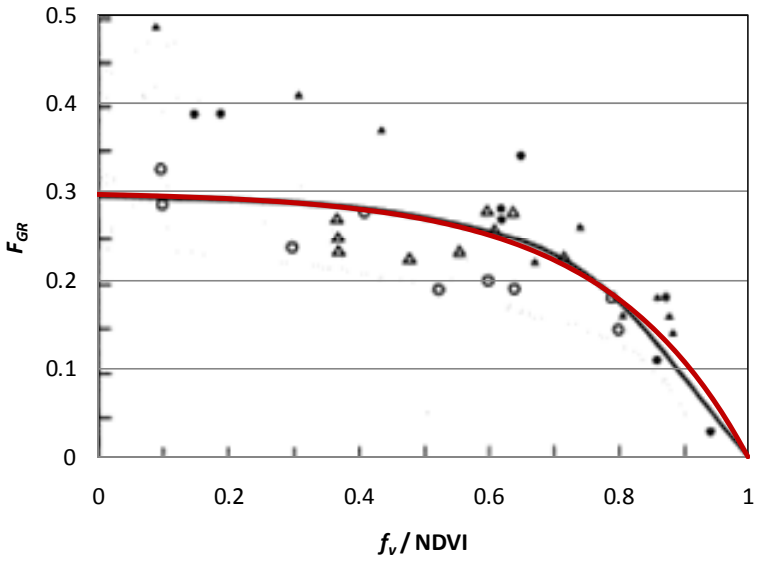

Figure 6. Polynomial relationship fitted to collated ground heat flux observations (Bastiaanssen *et al.* 1998) (black line and symbols, respectively) and Eq. [3-22] with visually fitted parameters ($F_{loss,max}$=0.30, $F_{s,ref}$ = 0.22).

3.8 Potential evaporation (E_0)

Equation

$$E_0 = f_{day} c_{RE} f_{E0} A_n \quad [3\text{-}23]$$

with

$$f_{E0} = \left(\frac{1}{1 + k_\varepsilon} \right) k_\alpha \quad [3\text{-}24]$$

$$k_\alpha = 1 + \frac{C_{aero} g_a}{A_n} \quad \text{(Penman-Monteith variant only)} \quad [3\text{-}25]$$

Variables

A_n daytime net available energy (W m^{-2})

E_0 potential evapotranspiration (mm d^{-1})

c_{RE} coefficient that converts energy flux (W m^{-2}) to equivalent water flux (mm d^{-1})

f_{E0} potential evaporative fraction (-)

k_α analogous Priestley-Taylor coefficient (variable in Penman-Monteith variant)

k_ε coefficient that determines evaporation efficiency

C_{aero} conversion factor that expresses the efficiency of aerodynamic energy use (J m^{-3})

g_a aerodynamic conductance (m s^{-1}) (cf. Section 3.9)

Parameters

k_α Priestley-Taylor coefficient (constant in Priestley-Taylor variant)

f_{day} fraction daylight hours (-)

Rationale

E_0 is defined here as the ET rate that would be expected from the land surface under ambient atmospheric conditions if the canopy and soil were wet. Common approaches to constraining the water balance by coupling to the energy balance tend to either (1) directly use meteorological variables in a surface model – normally a version of the Penman-Monteith combination equation (Monteith 1965) that directly couples energy and water fluxes; (2) define a potential evapotranspiration (PET) and scale this depending on water availability. Both require estimation of the radiation balance. The main difference is in the description of the coupling between the surface and the atmospheric boundary layer. A combination of the two approaches is followed here, which allows this coupling to be described explicitly if data on air humidity, wind speed and vegetation roughness are available, yet allows simplifying

assumptions to be used where they are not. The rationale and derivation of this approach is explained in Appendix A.3.

Parameter estimation

A number of simplifying assumptions can be made. In the simplest case, only A_n (required in Eq. [3-23] and T_{a*} (Eqs. [3-5] and [3-8]) are needed, in which case k_α is treated as a parameter, the Priestley-Taylor coefficient. The value of k_α is commonly estimated as 1.26, although higher values have been proposed to correct for vegetated surfaces with greater roughness (e.g. 1.32; Brutsaert and Stricker 1979; Morton 1983) and to estimate evaporation from well-watered areas experiencing considerable advection (up to 1.74; Jensen *et al.* 1990). Areas where advection is likely to occur include water bodies, wetlands and irrigated areas under dry, windy conditions. Alternatively, if data or good estimates of wind speed and vegetation roughness can be obtained, g_a can be estimated (Section 3.9) and therefore the P-M equation used.

3.9 Aerodynamic conductance (g_a)

Equations

$$g_a = k_{u2} u_2 \quad [3\text{-}26]$$

with

$$k_{u2} = \frac{0.305}{f(h)\left(f(h)+2.3\right)} \quad [3\text{-}27]$$

$$f(h) = \ln\left(\frac{813}{h} - 5.45\right) \quad [3\text{-}28]$$

Variables

u_2 effective wind speed at 2 m in climate stations (m s^{-1})

k_{u2} roughness coefficient for use with wind measurements at 2 m inside climate stations (-)

$f(h)$ function of h (-)

Parameters

h height of the vegetation canopy (m)

Rationale

These equation are based on the well-established theory proposed by Thom (1975). Their derivation is detailed in Appendix A.5.

Parameter estimation

The availability of accurate estimates of wind speed and canopy height are potentially important sources of uncertainty.

Detailed vegetation height data are not available at continental scale; instead values of 0.5 m and 10 m are assumed for short and tall vegetation (assumed equivalent to shallow- and deep-rooted vegetation, respectively).This produces k_{u2} and values of 0.0043 and 0.011 for short and tall vegetation, respectively. The former is close to the value of 0.0048 for a so-called FAO-56 reference grass (Allen *et al.* 1998).

For the default estimate of u_{2*}=3.5 m s^{-1} corresponding g_a values are 15 mm s^{-1} and 44 mm s^{-1} and these values are suggested as default values. Approaches to more accurately estimate g_a (or its components wind speed and vegetation roughness) would likely be a valuable enhancement for future model versions, however.

4. VAPOUR FLUXES

4.1 Water balance equations

The structure of the model component that estimates vapour fluxes is illustrated in Figure 7.

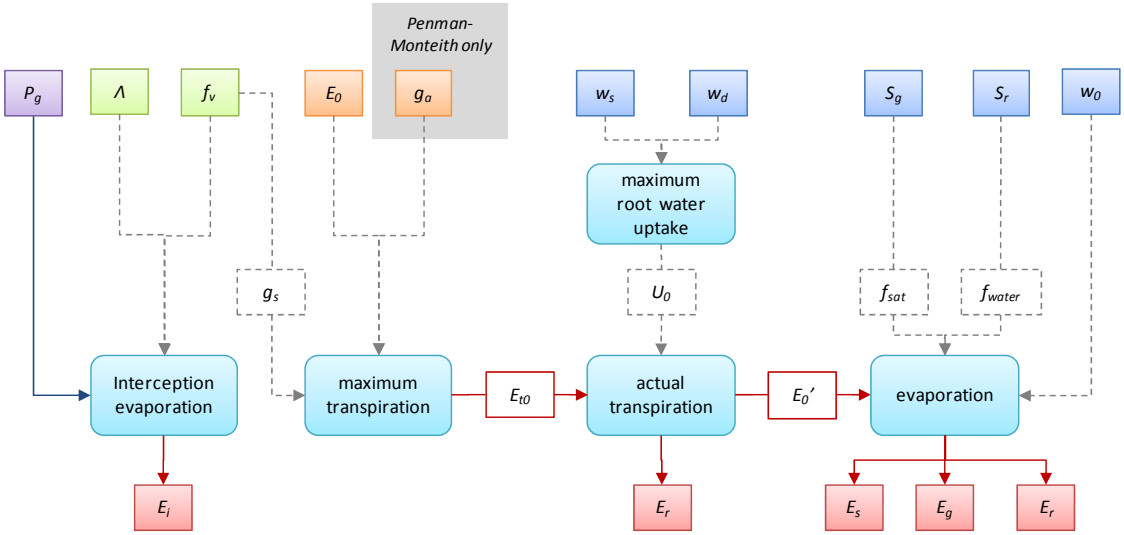

Figure 7. Flow diagram illustrating the module estimating vapour fluxes for a Hydrological Response Unit. Shown are the equations (cyan rounded boxes); vapour fluxes (red boxes); model input data (purple); variables simulated by the water balance module (blue; Section 2), radiation and energy balance module (orange; Section 3) and vegetation phenology module (green; Section 5). The grey shaded background shows a part of the model used only when the Penman-Monteith approach is applied.

Total evapotranspiration E is given by:

$$E = E_t + E_e = E_i + E_t + E_s + E_g + E_r \quad [4\text{-}1]$$

where E_t is transpiration and E_e is evaporation from all other sources, consisting of soil evaporation E_S, groundwater evaporation E_g (that is, evaporation from soil saturated by groundwater), open water evaporation E_r, and rainfall interception evaporation E_i.

Transpiration (E_t) is calculated in two steps: (1) maximum transpiration (E_{t0}; defined as the transpiration rate that would be achieved with unlimited root water supply) and maximum root water uptake (U_0) from all layers are estimated; (2) actual ET (E_t) is estimated as the lesser of the two. In formula:

$$E_t = \min\left[E_{t0}, U_0\right] \quad [4\text{-}2]$$

Further consistency between the sum of E_t and E_e (minus E_i) versus maximum available energy (by E_0) is ensured by calculating the energy available for evaporative fluxes ($E_{0'}$) as:

$$E_{0'} = E_0 - E_t \quad [4\text{-}3]$$

Note that this formulation still allows total ET to exceed PET for days with precipitation; this is deliberate (see Section 4.2). The equations used to estimate the constituent fluxes are explained below.

4.2 Rainfall interception evaporation (E_i)

Equations

$$E_i = f_V P_g \qquad \text{for } P < P_{wet} \qquad [4\text{-}4]$$

$$E_i = f_V P_{wet} + f_{ER}\left(P - P_{wet}\right) \qquad \text{for } P \geq P_{wet} \qquad [4\text{-}5]$$

with

$$P_{wet} = -\ln\left(1 - \frac{f_{ER}}{f_V}\right)\frac{S_V}{f_{ER}} \qquad [4\text{-}6]$$

$$S_V = s_{leaf}\Lambda \qquad [4\text{-}7]$$

$$f_{ER} = f_V F_{ER0} \qquad [4\text{-}8]$$

Variables

f_{ER}	ratio of average evaporation rate over average rainfall intensity during storms (-)
f_V	fraction area covered by intercepting leaves (-)
P_g	gross precipitation (mm)
P_{wet}	reference threshold rainfall amount at the canopy is wet (mm)
S_v	canopy rainfall storage capacity (mm)
Λ	leaf area index (-)

Parameters

F_{ER0}	specific ratio of average evaporation rate over average rainfall intensity during storms per unit canopy cover (-)
s_{leaf}	specific canopy rainfall storage capacity per unit leaf area (mm).

Rationale

The modelling approach used here is the widely adopted and evaluated event-based rainfall interception model of Gash (1979), with modifications made later by Gash *et al.* (1995) and Van Dijk and Bruijnzeel (2001a) to allow application to vegetation with a sparse canopy. One of the more important assumptions is that the ratio of wet canopy evaporation rate and rainfall intensity does not vary between storms. This assumption could be avoided if wet canopy evaporation rates could be accurately predicted and spatial and temporal rainfall intensity were available. Both are troublesome. It is commonly found that evaporation rates inferred from rainfall interception experiments exceed the energy estimated to be available from radiation and aerodynamic sources (e.g. Schellekens *et al.* 1999; Van der Tol *et al.* 2003; Murakami 2006; Wallace and McJannet 2006). Indeed, the assumption of constant interception fraction appears to hold up remarkably well, even for larger storms (which would be assumed to have, on

average, higher rainfall rates and therefore lower interception evaporation percentage-wise). Understanding the source of energy for the correspondingly high apparent evaporation rates is still an area of active research, but several mechanisms have been proposed that would effectively increase available energy to beyond that predicted by the Priestley-Taylor approach (see earlier references). For this reason, estimated interception evaporation is not subjected to the energy constraint of E_0, nor is available energy for the remaining evaporation fluxes (occurring during dry periods) reduced.

Because the physics of rainfall interception are not well understood, it is also as yet unclear to what extent wet canopy evaporation rates are influenced by canopy cover and density (see Van Dijk and Bruijnzeel 2001a for discussion). A conceptually simple assumption was made here, that evaporation rate is directly proportional to the fraction canopy cover.

Parameter estimation

Where direct event measurements of rainfall and canopy throughfall (as well as, preferably, stemflow) have been made, the specific relative evaporation rate f_{ER0} can be estimated by inversion of Gash-type models. This typically produces f_{ER0} ratios of 0.05 to 0.25, with values around 0.20 common (see reviews by Gash *et al.* 1995; Van Dijk and Bruijnzeel 2001b). Lower rates are reported for short, sparse vegetation in inland areas with intense rainfall (e.g. Llorens and Domingo 2007), whereas higher rates are often found with coastal forests receiving low intensity rainfall (Schellekens *et al.* 1999; Wallace and McJannet 2006). Values for f_{ER0} of 0.05 and 0.10 are used here as defaults for shallow- and deep-rooted vegetation, as these are assumed by and large equivalent with aerodynamically smooth and rough vegetation, respectively.

Values for s_{leaf} that can be calculated from literature are 0.07–0.6 mm per unit LAI for most forests types, and 0.03–0.9 mm for low vegetation (see review in Van Dijk and Bruijnzeel, 2001b). Leaf size and smoothness are important factors determining water holding capacity. Most reported values are around 0.10 mm and this is therefore used as a default value for both HRUs.

4.3 Maximum transpiration (E_{t0})

Equations

$$E_{t0} = f_t E_0 = E_0 \Big/ \left[1 + \left(\frac{k_\varepsilon}{1 + k_\varepsilon} \right) \frac{g_a}{g_s} \right] \qquad [4\text{-}9]$$

with

$$f_t = \left[1 + \left(\frac{k_\varepsilon}{1 + k_\varepsilon} \right) \frac{g_a}{g_s} \right]^{-1} \qquad [4\text{-}10]$$

$$g_s = f_V G_{s\max} \qquad [4\text{-}11]$$

Variables

E_{t0}	maximum transpiration (mm d^{-1})
E_0	potential evapotranspiration (mm d^{-1})
f_t	potential transpiration fraction (-)
f_V	fraction canopy cover (-)
g_a	aerodynamic conductance (m s^{-1}) (cf. Section 3.9)
g_s	canopy conductance (m s^{-1})
k_ε	coefficient that determines evaporation efficiency (cf. Section 3.1)
Λ	leaf area index (-)

Parameter

G_{smax}	maximum stomatal conductance per unit canopy cover (m s^{-1}).

Rationale

This relationship is in accordance with the Penman-Monteith combination equation, and is derived in Appendix A. For a closed canopy, g_s can be thought of as a function of maximum surface conductance (G_{smax} in m s^{-1}) and a scaling factor (between zero and unity) that describes the reduction in surface conductance as a consequence of stomatal control. Various alternative formulations have been developed to describe stomatal control as a function of ambient conditions inside the vegetation, the air around the vegetation and/or the soil water status. However many of these formulations were based on interpretation of real world, small scale experiments where correlation between potential driving factors is inevitable, due to the diurnal cycles in many atmospheric and plant physiological variables; correlation between soil water availability and atmospheric humidity; and surface-atmosphere feedback effects (e.g. Jarvis and McNaughton 1986; Jones 1998). The strongest control appears to be the down regulation of g_s when leaf water potential decreases. Controlled experiments suggest that this is primarily

caused by the difference between soil water uptake and transpiration rate (Jones 1998), which is already accounted for separately in the estimation of actual transpiration (Section 4.1). Other potential direct effects of atmospheric conditions on stomatal conductance may be more important on sub-daily basis but not have much influence on daily average values.

Parameter estimation

The fraction vegetation is simulated by the model and therefore the only parameter that requires estimation is G_{smax}. Surface conductance g_s is estimated at 15 mm s^{-1} for a FAO-56 reference grass cover (Allen *et al.* 1998). Other studies typically find maximum g_s values of 10 to 20 mm s^{-1}, with values of more than 30 mm s^{-1} for agricultural crops (Kelliher *et al.* 1995; Leuning *et al.* 2008).

Corresponding to functional convergence theory, it has been shown that there is correlation between canopy photosynthetic capacity, surface conductance, specific leaf area and other plant physiological properties (Reich *et al.* 1997; 2003). Remotely sensed indices such as NDVI and EVI have been shown to correlate well and approximately linear with both photosynthetic capacity and surface conductance. The variation in g_s between vegetation types and over time would therefore be expected to correlate well with the variation in these indices, allowing the use of remote sensing observations to estimate g_s.

Particularly useful is the Enhanced Vegetation Index, which has been shown better correlated to canopy photosynthetic capacity than previous vegetation indices such as FPAR and NDVI (Huete *et al.* 2002). A satellite-based specific photosynthetic capacity index (PCI, expressed per unit canopy cover) can be calculated from EVI and FPAR (as an estimate of f_V) using the method described in AWRA Background Report 2010/3 (Van Dijk and Warren 2010). This produced PCI values of 0.5-1.0 for humid tropical vegetation and greening inland grassland areas, whereas forests typically showed a PCI of 0.30-0.45. PCI values of 0.35 and 0.65 were used as estimates in the current model version, but improvements to incorporate spatially explicit information will be considered for future versions. Comparing these with earlier mentioned G_{smax} values suggests that it may be estimated as:

$$G_{s\max} = 0.03PCI \qquad [4\text{-}12]$$

4.4 Root water uptake (U_0)

Equations

$$U_0 = \max[U_{S0}, U_{D0}] \quad [4\text{-}13]$$

with U_{Smax} and U_{Dmax} both estimated as:

$$U_{z0} = U_{z\max} \min\left(1, \frac{w_z}{w_{z\lim}}\right) \quad [4\text{-}14]$$

where subscript '*z*' is to be replaced by '*s*' and '*d*', respectively.

Variables

U_0 maximum root water uptake under ambient conditions (mm d^{-1})

U_{zmax} physiological maximum root water uptake from layer *z* (mm d^{-1})

U_{z0} maximum root water uptake rates from layer *z* under ambient conditions (mm d^{-1})

w_z relative water content of layer *z*

Parameters

w_{zlim} uptake-limiting relative water content in layer *z*

Rationale

The formulation used here is intended to be one of the simplest ways in which root water uptake can be expressed, while still recognising two important limitations on root water uptake: the effect of soil water availability in different layers; and that of root presence and hydraulic properties in different layers. The description used is very similar to other approaches to estimate the impact of soil water content on root water uptake (see Shuttleworth 1992 for examples). Some approaches estimate limitation on the basis of soil matric potential; others on the basis of water content. Most produce factors by which maximum transpiration is scaled regardless of its magnitude, rather than comparing the relative magnitude of demand and supply directly.

The approach used here was chosen due to the high complexity of root water uptake when considering the scale of modelling, the very high spatial variability in soil properties, soil moisture availability and vegetation rooting depth, and the differences in rooting pattern and physiology between plants of different species and age. More complex approaches exist, such as the detailed process models of the transient dynamics of pressure differentials (e.g. Tuzet *et al.* 2003; Schymanski *et al.* 2008). Since a unique relationship between matrix potential and water content is always assumed (that is, any hysteresis in the soil moisture retention or 'pF' curve is ignored), one can be expressed in terms of the other and the only difference will be in the exact shape of the limitation function. Given the uncertainty in the parameters, and given that it is unlikely that robust estimates of the parameters can be derived and therefore would need to be calibrated, a formulation with a minimum number of two additional parameters was chosen.

Parameter estimation

The maximum root water uptake U_{z0} would be expected to depend on the total length of fine roots, the flow resistance from roots to leaf, and the potential difference between plant and soil. There are currently no methods to estimate maximum uptake rates, but site water use observations by flux towers suggest that maximum daily transpiration rates do not normally seem to exceed around 6 mm d^{-1} and drop to a relatively constant 1 or 2 mm d^{-1} for deep rooted vegetation after seasonal vegetation has senesced (cf. AWRA Technical Report 4). These observations were used to estimate default values for U_{S0} and U_{D0} of 6 and 2 mm d^{-1}, respectively.

The water content w_{zlim} at which root water uptake is affected can be assumed to be between 0.15 and 0.50 based on available pedotransfer functions (Table 1; Rawls *et al.* 1992; Shuttleworth 1992). This value is suggested as default value. Note that w_{zlim} is expressed here somewhat differently than in many published cases, since any water that remains after root water uptake has ceased altogether is ignored in the definition of field capacity used here. Actual values will depend, among others, on soil texture and constituents but also on the matric potential that can be overcome by plant roots; this potential value is greater for plants that tolerate drought (e.g. Tyree 1999). It is also noted that within the model the parameter w_{zlim} behaves as an effective parameter in which the heterogeneity in the soil properties and plant root distribution is implicit.

Table 1. Indicative estimates of uptake limiting soil water content based on some published 'average' soil properties (Table 5.3.2 in Rawls *et al.* 1992) and the assumption that water becomes limiting at 50-80% of field capacity (cf. Shuttleworth 1992).

	Vol% at wilting point	Vol% at field capacity	w_{lim} (range)	
sand	3.3	9.1	0.32	0.51
sandy loam	9.5	20.7	0.27	0.43
clay loam	19.7	31.8	0.19	0.30
clay	27.2	39.6	0.16	0.25

4.5 Soil evaporation (E_s)

Equations

$$E_s = (1 - f_{sat} - f_{water}) f_{sE} (E_0 - E_t) \quad [4\text{-}15]$$

with

$$f_{sE} = F_{sE\max} \min\left\{1, \frac{w_0}{w_{0\lim}}\right\} \quad [4\text{-}16]$$

Variables

E_0 potential ET (mm d^{-1})

E_t actual transpiration (mm d^{-1})

f_{sat} fraction area covered by saturated soil (-)

f_{water} fraction area covered by open water (-)

f_{sE} relative soil evaporation (-)

w_0 relative top soil water content (-)

Parameters

F_{sEmax} relative soil evaporation when soil water supply is not limiting (-)

w_{0lim} relative top soil water content at which evaporation is reduced (-)

Rationale

Existing models to describe evaporation from areas of bare soil usually consider evaporation to occur in three stages (e.g. Ritchie 1972; Allen *et al.* 2005): (1) evaporation from wet soil occurs at a rate that is approximately equal to PET; (2) once soil wetness falls below a certain threshold, evaporation is reduced and becomes increasingly reduced as soil moisture decreases further; and (3) below a certain water content soil evaporation ceases altogether. Mutziger *et al.* (2005) did a global review of published data sets and found that this approach produces realistic soil evaporation estimates.

An important source of uncertainty is that the models commonly used to describe soil evaporation have been derived mostly from studies on bare fields or lysimeters within the context of agricultural water use estimation. Where litter, vegetation or other forms of non-evaporating material cover part of the soil, they will intercept radiation energy as well as increase surface roughness, and so reduce evaporation from the underlying soil. In addition, plant root systems can facilitate the transfer of deeper soil moisture to shallow soil, particularly when the top soil is very dry, through hydraulic redistribution (e.g. Richards and Caldwell 1987; Burgess *et al.* 1998; Zou *et al.* 2005). As a consequence, top soil moisture content under living vegetation is unlikely to fall much below wilting point. More complex models exist, such as the Shuttleworth-Wallace sparse canopy model; an elaboration of the Penman-Monteith

model (Shuttleworth and Wallace 2007). However, to be beneficial, this type of models requires additional data on canopy structure and configuration as well as wind speed and humidity. Accurate observations of these variables are not available over large areas and therefore the much simpler model used here was chosen. It is comparable to the formulation used for root water uptake and combines the second and third phase of soil dry down into a single phase. This is done partly for convenience and simplicity, and partly because capillary rise and hydraulic redistribution by vegetation may well prevent this third phase from being reached. The soil moisture depletion curve produced by the equation used here is similar to that produced by the FAO recommended method (Allen *et al.* 2005) if the average parameters reported by Mutziger et al (2005) are used, as shown in Figure 8.

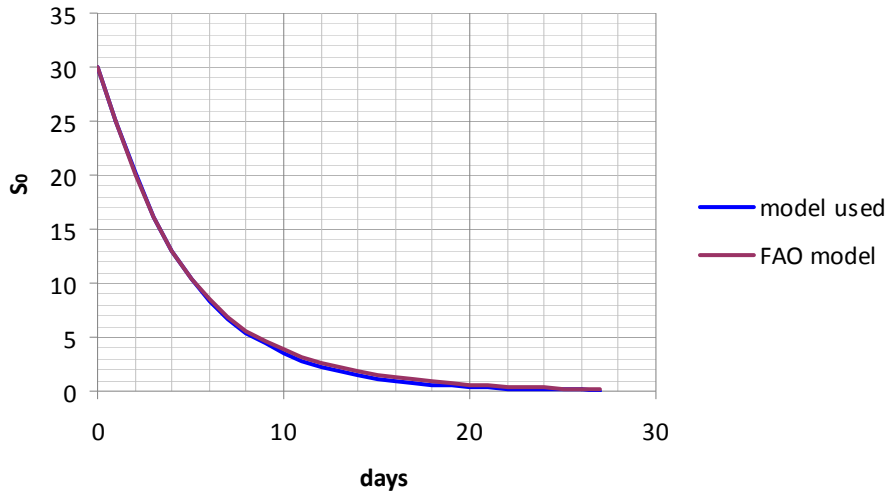

Figure 8. Soil dry down curve produced with the FAO method (red line) and produced by the model used here (blue line). Parameters for the FAO method are 5, 20 and 5 mm for the 'available water' in each of the three stages and 0.17 for 'relative evaporation rate' (rounded median values from the experiments reported by Mutzinger *et al.*, 2005). Parameters for the method used here re S_{0FC}=30 mm and w_{0lim}=0.85. Both are for a hypothetical potential ET of 5 mm d^{-1}.

Parameter estimation

The relative soil evaporation when soil water supply is not limiting (F_{sEmax}) is commonly assumed approximately equal or slightly higher than unity when E_0 is estimated as FAO crop reference ET (Allen *et al.* 1998). Here the available energy for soil evaporation is defined by the difference between Priestley-Taylor PET and actual transpiration. Therefore F_{sEmax} defines the efficiency with which energy not used for transpiration is transferred to the soil, and the degree to which water vapour is efficiently transported from the soil surface to the atmosphere. A value less than unity would be expected where there is some vegetation cover, litter or other forms of surface cover that impedes energy to, or vapour fluxes from, the wet soil. A value of F_{sEmax}=0.7 is estimated as a default, but it should be noted that this value is without much experimental support. Where rainfall occurs infrequently (e.g. arid environments), the assumed value is not expected to introduce bias, as the soil will have sufficient time to dry out between storms.

The relative top soil water content at which evaporation is reduced w_{0lim} may be expected to be somewhat higher than that at which root water uptake stops. Indeed, from the five studies

reviewed by Mutziger *et al.* (2005), w_{0lim} values of 0.60 to 0.89 can be calculated, with a median of 0.84. This is higher than the 0.15 to 0.50 suggested for root water uptake, as would be expected (Section 4.4). Conversely, soil evaporation may reduce soil water content to below wilting point, particularly in fine textured soils. In the model structure this can be accounted for by increasing the storage at field capacity S_0 and increasing the value of w_{0lim} by perhaps up to 5%. A default value of w_{0lim}=0.85 is suggested here.

Mutziger *et al.* (2005) estimate the maximum available water storage for soil evaporation at 18 to 50 mm for the five studies reviewed, with an average of ca. 30 mm.

4.6 Groundwater evaporation (E_g)

Equation

$$E_g = f_{sat} F_{sE\max} \left(E_0 - E_T \right) \qquad [4\text{-}17]$$

Variables

E_g groundwater evaporation (mm d^{-1})

E_0 potential ET (mm d^{-1})

E_t actual transpiration (mm d^{-1})

f_{sat} fractions of area covered by saturated soil

Parameters

F_{sEmax} soil evaporation scaling factor when soil water supply is not limiting evaporation

Rationale

The model used here is the same as that used for unsaturated soil evaporation for the condition that w=1.

Parameter estimation

The scaling factor F_{Emax} has the same meaning as that used for unsaturated soil evaporation (Section 4.5). The same default value is suggested.

4.7 Open water evaporation (E_r)

Equation

$$E_r = f_{water} F_{ow} \left(E_0 - E_T \right) \quad [4\text{-}18]$$

with

$$f_{water} = \min\left(F_{bankfull}, 0.007 S_r^{0.75} \right) \quad [4\text{-}19]$$

Variables

E_r surface water evaporation (mm d^{-1})

E_0 potential ET (mm d^{-1})

E_t actual transpiration (mm d^{-1})

f_{water} fraction of area covered by water (-)

S_r streamflow storage (mm)

Parameters

F_{0w} open water evaporation scaling factor (-)

$F_{bankfull}$ fraction river channel at bank-full capacity (-)

Rationale

The model formulation used is consistent with those used for the other evaporation components. The value of f_{water} would be expected to change dynamically in response to the volume of water stored in surface water bodies. There are currently no accurate predictive models available, and it may be expected that any relationship would vary between landscapes with different drainage network morphology. Based on studies of small and large, natural and man-made reservoirs (e.g. Lowe *et al.* 2005) as well as geometric considerations, the exponent of the empirical equation may be estimated to be between 0.5 and 1.0; a value of 0.75 is estimated based on the work by Lowe *et al.* (2005) for hillside farm dams and used as a default value. Based on the same study a value of 0.007 mm^{-1} was estimated for the coefficient (that is, f_{water}=0.7% of the landscape for S_r=1 mm).

It is further assumed that some surface water will remain in the river channel and water holes after flow ceases altogether, and will remain to be gradually evaporated over the course of time, creating a 'negative' water storage (that is, the river channel will need to be wetted before streamflow occurs again). The fraction of area occupied by river channels ($F_{bankfull}$) is unknown, but is estimated here as 0.5% of the landscape.

Simple scaling of PET is commonly applied to estimate open water evaporation rates. Models exist that describe the physics of radiation absorption and heat storage, which can influence open water evaporation (De Bruin 1982). However attempts to use such methods need to account for the depth of the water column and the temperature of water inflows, both of which are highly variable and poorly known. A comparison by McJannet *et al.* (2008) for open water

bodies in the Murray-Darling Basin suggested that heat storage can have considerable influence on evaporation rates from day to day (cf. Roderick *et al.* 2009), however they also found that for longer periods (e.g. a month) the use of a constant scaling factor appears to perform just as well.

Parameter estimation

The open water evaporation coefficient F_{0w} is assumed to be equal to the conversion factor between potential evaporation and pan evaporation, which is usually estimated at 0.70 but varies depending on pan configuration and environmental conditions (Shuttleworth 1992; Roderick *et al.* 2009). Uncertainty for larger surface water bodies occurs because of inflow of water with a different temperature, water depth and stratification, energy advection, and effects of riparian vegetation on aerodynamic conductance. A range of 0.6 to 0.8 may cover most of these effects (McJannet *et al.* 2008); as a default value 0.7 is used.

5. VEGETATION PHENOLOGY

5.1 Introduction

The vegetation phenology[9] model simulates canopy changes in response to water availability by calculating the vegetation cover that could be sustained given soil moisture availability. The 'equilibrium' leaf mass is estimated by considering the hypothetical leaf mass M_{eq} that corresponds with a situation in which maximum transpiration rate ($E_{t,max}$) equals maximum root water uptake (U_{max}). The vegetation moves towards this equilibrium state with a prescribed degree of inertia, representative of alternative phenological strategies.

The model can include one or more land cover types, each defined by their fractional cover and properties. Currently, two land cover types are considered: deep- and shallow-rooted vegetation. It is assumed, compared to shallow-rooted vegetation, deep-rooted vegetation has a longer leaf life span, responds less rapidly to changes in water availability, and has lower photosynthetic capacity and stomatal conductance per unit leaf area. These expectations can be derived from functional convergence theory and agrees with observed relationships (Reich *et al.* 1997; Wright *et al.* 2004).

To minimise complexity, only the effects of water availability on vegetation phenology is considered in the current model version, as these most likely will have the greatest influence on hydrological processes. However, other processes may regionally be more important in driving vegetation phenology, in particular in the humid and high elevation regions of southern Australia where temperature and day length are important variables driving vegetation phenology (see AWRA Technical Report 4). Moreover, growth limiting factors such as nutrient availability and salinity may impose an upper limit on the vegetation density that can be sustained. Further refinement of the model will be considered but needs to consider the degree to which these factors and processes help improve water balance estimates.

5.2 Mass balance equation

$$M_L(t+1) = M_L(t) + m_{Ln}(t) \qquad [5\text{-}1]$$

where M_L is the biomass and m_{Ln} the net biomass change of living leaves (both expressed in kg dry matter per m^2). The coupling with water balance dynamics occurs through m_{Ln} (Section 5.4).

5.3 Conversion equations

Equations

$$f_V = 1 - \exp\left(-\frac{\Lambda}{\Lambda_{ref}}\right) \qquad [5\text{-}2]$$

[9] *phenology*: relating to cyclical biological events in response to climatic conditions, in particular greening and senescence in response to water availability.

$$\Lambda = M_L C_{SLA} \quad [5\text{-}3]$$

Variables

f_V canopy fractional cover

Λ leaf area index

Parameters

Λ_{ref} reference leaf are index (at which f_V=0.63)

C_{SLA} specific leaf area (m^2 kg^{-1})

Rationale

The conversion between M_L and Λ is strictly a dimensional one. It assumes that, by good approximation, the value of the coefficient of proportionality that is specific leaf area C_{SLA} does not vary significantly over time for a particular vegetation type. This is a common assumption but obviously a simplification.

The conversion from Λ to f_V is described by the exponential light extinction equation (Monsi and Saeki 1953) equivalent to Beer's Law which is most commonly used for this purpose. However to be consistent with notation elsewhere in the model, the so-called 'light extinction coefficient' (often symbolised by κ) is not used but its inverse value Λ_{ref}, which represents a reference LAI at which fraction cover is 0.632. Use of the Monsi-Saeki model assumes that reference LAI (or κ) does not change over time, which is a necessary simplification. It should be noted that Λ_{ref} is a function of wavelength, leaf angle distribution and light incidence angle, or angle distribution in the case of diffuse radiation. Because f_V is primarily used to estimate light interception integrated over the day, Λ_{ref} is also best interpreted as a radiation-weighted effective value.

Parameter estimation

Globally reported values of C_{SLA} vary by two orders of magnitude, from 0.7 to 71 m^2 kg^{-1} (Wright *et al.*, 2004). Values of 1.5 to 9 m^2 kg^{-1} have been found for Australian Eucalypt species (Schulze *et al.* 2006) with an average value of ca. 3 m^2 kg^{-1}.

Literature reported Λ_{ref} values are usually in the range of 1.3 to 2.5 (κ =0.4–0.8). Higher Λ_{ref} values correspond with more vertical leaf angles; for Eucalypt forests, values of 1.8 to 2.0 (κ=0.50–0.55) are commonly estimated, whereas values as high as 4.2–7.1 (κ=0.14-0.24) have been estimated for zenith incidence angles (Macfarlane *et al.* 2007). Values of Λ_{ref} can also be derived directly from MODIS satellite LAI and FPAR products, if it is assumed that FPAR is a good approximation of canopy cover f_V. Preliminary research into this is reported in AWRA Background Paper 2010/3 (Van Dijk and Warren 2010), which found higher values of Λ_{ref} in areas dominated by tree cover. For areas with high persistent FPAR (equivalent to forest vegetation) an average Λ_{ref} value of 2.5 (κ=0.40) was calculated, whereas for areas with low persistent FPAR a Λ_{ref} =1.4 (κ=0.70) is derived. These values were used for respectively deep-rooted and shallow-rooted vegetation in the model. A caveat is that these results will be influenced, but to an unknown degree, by spurious influences from the assumptions and observations used in the derivation of the products.

5.4 Net leaf biomass change (m_{Ln})

Equations

$$m_{Ln} = \frac{M_{Leq} - M_L}{t_{grow}} \qquad \text{if } M_{Leq} \geq M \qquad [5\text{-}4]$$

$$m_{Ln} = \frac{M_{Leq} - M_L}{t_{senesence}} \qquad \text{if } M_{Leq} < M \qquad [5\text{-}5]$$

Variables

M_{Ln} net leaf biomass change (kg m^{-2} d^{-1})

M_{Leq} equilibrium dry leaf biomass given water availability and atmospheric demand (kg m^{-2})

M_L dry leaf biomass (kg m^{-2})

Parameters

t_{grow} characteristic time scale for vegetation growth towards equilibrium (days)

$t_{senesce}$ characteristic time scale for vegetation senescence towards equilibrium (days)

Rationale

The formulation used here was newly developed, because literature review did not suggest a suitably simple model that predicts water-related vegetation phenology (see review by Arora 2002). The formulation is based on the assumption that vegetation is able to adjusts is leaf biomass at a rate that is independent of the amount of existing leaf biomass and energy or biomass embodied in other plant organs. The approach shows good performance for dynamic, typically shallow-rooted, vegetation in seasonally dry environments. As would be expected, its predictive performance is lesser for deep rooted vegetation, particularly in areas where temperature or radiation and not water are the most growth limiting resource (AWRA Technical Report 4).

The model is obviously a strong simplification of a complex physiological process. In reality, the initial stages of canopy expansion may be constrained by the availability and ability to mobilise energy and matter from other plant organs, whereas in the later stages of canopy expansion growth rates may become limited by antecedent photosynthetic assimilation. Therefore, it may be that explicit consideration of the biomass balance leads to better simulation of vegetation phenology. This would require explicit estimation of all assimilation and respiration fluxes from all vegetation organs explicitly and would inevitably involve several more parameters and assumptions. The benefit of a more complex treatment of vegetation phenology should be considered for future model versions.

Parameter estimation

There are limits to the rate at which vegetation will grow and contract its canopy in response to soil water availability, with deep-rooted vegetation adjusting slower to increases in water availability than does shallow-rooted vegetation. Furthermore, downward adjustment may occur at a rate that is different from upward adjustment. There is little information available in the literature to estimate t_{grow} and $t_{senensce}$ from. However, they can readily be calibrated to LAI patterns derived from remote sensing. Through visual estimation for around 30 sample locations across Australia, t_{growth} and $t_{senesce}$ were both estimated at 50 days for shallow-rooted vegetation, and 90 days for deep-rooted vegetation. Further improvements are likely to be possible through more elaborate calibration and model-data fusion approaches in future.

5.5 Equilibrium leaf biomass (M_{Leq})

$$M_{Leq} = -\ln(1 - f_{Veq})\frac{\Lambda_{ref}}{C_{SLA}} \quad [5\text{-}6]$$

with

$$f_{Veq} = \frac{1}{\frac{E_0}{U_0} - 1}\left(\frac{k_\varepsilon}{1 + k_\varepsilon}\right)\frac{g_a}{G_{s\max}} \quad \text{for } f_{Veq} < f_{Vmax} \quad [5\text{-}7]$$

$$f_{Veq} = f_{V\max} \quad \text{for } f_{Veq} \geq f_{Vmax} \quad [5\text{-}8]$$

and

$$f_{V\max} = 1 - \exp\left(-\frac{\Lambda_{\max}}{\Lambda_{ref}}\right)$$

Variables

E_0 potential evapotranspiration (mm d^{-1})

f_V fraction canopy cover (-)

f_{Vmax} maximum achievable canopy cover (-)

g_a aerodynamic conductance (m s^{-1})

g_s canopy conductance (m s^{-1})

k_ε coefficient that determines evaporation efficiency (-)

M_{Ln} net leaf biomass change (kg m^{-2} d^{-1})

M_{Leq} equilibrium dry leaf biomass given water availability and atmospheric demand (kg m^{-2})

U_0 maximum root water uptake (mm d^{-1})

Parameters

G_{smax} maximum stomatal conductance per unit canopy cover (m s^{-1}).

Λ_{max} maximum achievable leaf area index (-)

Λ_{ref} reference leaf area index (-)

Rationale

The approach adopted here is newly developed based on some simple assumptions. It follows from the principle of optimum resource use, which implies that leaf area will adjust - within the limits of plant physiology and resource availability - to bring transpiration rates in equilibrium with the capacity of the roots to draw water from the soil (U_{max}). The corresponding equilibrium fractional vegetation cover is defined by (cf. Section 4.3):

$$U_0 = f_t E_0 = \frac{E_0}{1 + \left(\frac{k_\varepsilon}{1 + k_\varepsilon}\right)\left(\frac{g_a}{f_{Veq} g_{s\max}}\right)} \quad [5\text{-}9]$$

The equilibrium approach has been shown to perform well in reproducing satellite-observed vegetation greenness patterns, particularly for seasonal vegetation that responds to water availability pulses (Van Dijk and Renzullo 2009). Opportunities to improve the approach may be considered in future versions.

Parameter estimation

Methods to estimate Λ_{ref} and G_{smax} are provided in Sections 4.3 and 5.3, respectively.

The parameter Λ_{max} is introduced to replicate the limiting effect of maintenance respiration losses in the maximum leaf area that can be sustained. Maximum LAI values found in Australia generally appear to be less than 7 for eucalypt forests, although values of up to 10 have been reported for agricultural crops (Hill *et al.* 2006). Globally, even higher values have been reported for humid forests, plantations and wetlands (Asner *et al.* 2003). A value of Λ_{max}=8 is used as a default in the model. It is noted that this parameter will not normally have much influence on ET estimation, as water availability and growth rate will limit the LAI that can be achieved in water limited environments; whereas available energy rather than LAI will determine ET in energy-limited environments.

REFERENCES

Allen RG, Pereira LS, Raes D, Smith M (1998) 'Crop evapotranspiration - Guidelines for computing crop water requirements.' Food and Agricultural Organisation of the United Nations, Rome.

Allen RG, Pereira LS, Smith M, Raes D, Wright JL (2005) FAO-56 dual crop coefficient method for estimating evaporation from soil and application extensions. *Journal of irrigation and drainage engineering* **131**, 2.

Arora V (2002) Modeling vegetation as a dynamic component in soilvegetation-atmosphere transfer schemes and hydrological models. *Reviews of Geophysics* **40**, 1006.

Asner G, Scurlock J, Hicke J (2003) Global synthesis of leaf area index observations: implications for ecological and remote sensing studies. *Global Ecology and Biogeography* **12**, 191-205.

Bastiaanssen WGM, Menenti M, Feddes RA, Holtslag AAM (1998) A remote sensing surface energy balance algorithm for land (SEBAL). 1. Formulation. *Journal of Hydrology* **212**, 198-212.

Benyon RG (1999) Nighttime water use in an irrigated Eucalyptus grandis plantation. *Tree Physiology* **19**, 853.

Bergström S, Singh VP (1995) The HBV model. *Water Resources Publications*, 443-476.

Beven KJ (2004) 'Rainfall-runoff modelling: the primer.' (John Wiley & Sons Inc

Bouma J (1989) Using soil survey data for quantitative land evaluation. *Advances in Soil Science* **9**, 177–213.

Brutsaert W (1975) On a derivable formula for long-wave radiation from clear skies. *Water Resources Research* **11**, 742-744.

Brutsaert W (1982) 'Evaporation into the atmosphere: theory, history, and applications.' (D Reidel Pub Co

Brutsaert W, Stricker H (1979) An advection-aridity approach to estimate actual regional evapotranspiration. *Water Resources Research* **15**, 443-450.

Burgess SSO, Adams MA, Turner NC, Ong CK (1998) The redistribution of soil water by tree root systems. *Oecologia* **115**, 306-311.

Burnash RJC, Ferral RL, McGuire RA (1973) 'A generalized streamflow simulation system: conceptual models for digital computers, J.' Joint Federal-State River Forecast Center, Sacramento, California.

Chiew FHS, Peel MC, Western AW (2002) Application and testing of the simple rainfall-runoff model SIMHYD. In 'Mathematical Models of Small Watershed Hydrology and Applications '. (Eds VP Singh and DK Frevert) pp. 335-367. (Water resources Publication Littleton, Colorado, USA)

Dawson TE, Burgess SSO, Tu KP, Oliveira RS, Santiago LS, Fisher JB, Simonin KA, Ambrose AR (2007) Nighttime transpiration in woody plants from contrasting ecosystems. *Tree Physiology* **27**, 561.

De Bruin HAR (1982) Temperature and energy balance of a water reservoir determined from standard weather data of a land station. *Journal of Hydrology* **59**.

Duarte HF, Dias NL, Maggiotto SR (2006) Assessing daytime downward longwave radiation estimates for clear and cloudy skies in Southern Brazil. *Agricultural and Forest Meteorology* **139**, 171-181.

Dunkerley D (2002) Systematic variation of soil infiltration rates within and between the components of the vegetation mosaic in an Australian desert landscape. *Hydrological Processes* **16**, 119-131.

Gash JHC (1979) An analytical model of rainfall interception by forests. *Quarterly Journal of the Royal Meteorological Society* **105**, 43-55.

Gash JHC, Lloyd CR, Lachaud G (1995) Estimating sparse forest rainfall interception with an analytical model. *Journal of Hydrology* **170**, 79-86.

Guerschman J-P, Van Dijk AIJM, McVicar TR, Van Niel, T.G., Li L, Liu Y, Peña-Arancibia J (2008) 'Water balance estimates from satellite observations over the Murray-Darling Basin.' CSIRO, Canberra, Australia.

Guerschman JP, Van Dijk A, Mattersdorf G, Beringer J, Hutley LB, Leuning R, Pipunic RC, Sherman BS (2009) Scaling of potential evapotranspiration with MODIS data reproduces flux observations and catchment water balance observations across Australia. *Journal of Hydrology* **369**, 107-119.

Hill M, Senarath U, Lee A, Zeppel M, Nightingale J, Williams R, McVicar T (2006) Assessment of the MODIS LAI product for Australian ecosystems. *Remote Sensing of Environment* **101**, 495-518.

Hobbins MT, Ramírez JA, Brown TC (2001) The complementary relationship in estimation of regional evapotranspiration: An enhanced advection-aridity model. *Water Resources Research* **37**, 1389–1403.

Huete A, Didan K, Miura T, Rodriguez EP, Gao X, Ferreira LG (2002) Overview of the radiometric and biophysical performance of the MODIS vegetation indices *Remote Sensing of Environment* **83**, 195-213.

Jakeman AJ, Hornberger GM (1993) How much complexity is warranted in a rainfall-runoff model? *Water Resources Research* **29**, 2637–2649.

Jarvis PG, McNaughton KG (1986) Stomatal control of transpiration: scaling up from leaf to region. *Advances in ecological research* **15**, 1-49.

Jeffrey SJ, Carter JO, Moodie KB, Beswick AR (2001) Using spatial interpolation to construct a comprehensive archive of Australian climate data. *Environmental Modelling and Software* **16**, 309-330.

Jensen ME, Burman RD, Allen RG (1990) 'Evaporation and irrigation water requirements. .' American Society of Civil Engineers, New York, USA

Jones CG, Lawton JH, Shachak M (1997) Positive and negative effects of organisms as physical ecosystem engineers. *Ecology* **78**, 1946-1957.

Jones D, Wang W, Fawcett R (2009) High-quality spatial climate data-sets for Australia. *Australian Meteorological and Oceanographic Journal*.

Jones DA, Wang W, Fawcett R (2007) 'Climate data for the Australian Water Availability Project, Final Milestone Report.'

Jones HG (1998) Stomatal control of photosynthesis and transpiration. *Journal of Experimental Botany* **49**, 387-398.

Kelliher FM, Leuning R, Raupach MR, Schulze ED (1995) Maximum conductances for evaporation from global vegetation types *Agricultural and Forest Meteorology* **73**, 1-16.

King EA, Paget MJ, Briggs PR, Raupach MR, Trudinger CM (in press) Operational Delivery of Hydrometeorological Monitoring and Modelling over the Australian Continent. *IEEE Journal Of Selected Topics In Earth Observations And Remote Sensing*.

Kirby JM, Van Dijk AIJM, Mainuddin M, Peña-Arancibia J, Guerschman JP, Liu Y, Marvanek S, McJannet DL, Paydar Z, McVicar TR, Van Niel TG, Li LT (2008) 'River water balance accounts across the Murray-Darling Basin, 1990-2006.' CSIRO, Canberra, Australia.

Kowalczyk EA, Wang YP, Law RM, Davies HL, McGregor JL, Abramowitz G (2006) 'The CSIRO Atmosphere Biosphere Land Exchange (CABLE) model for use in climate models and as an offline model.' CSIRO Marine and Atmospheric Research.

Ladson T, Lander J, Western A, Grayson RB (2004) 'Estimating extractable soil moisture content for Australian soils.' CRC Catchment Hydrology, Canberra.

Leuning R, Zhang YQ, Rajaud A, Cleugh H, Tu K (2008) A simple surface conductance model to estimate regional evaporation using MODIS leaf area index and the Penman-Monteith equation. *Water Resources Research* **44**, W10419.

Lindström G, Johansson B, Persson M, Gardelin M, Bergström S (1997) Development and test of the distributed HBV-96 hydrological model. *Journal of Hydrology* **201**, 272-288.

Llorens P, Domingo F (2007) Rainfall partitioning by vegetation under Mediterranean conditions. A review of studies in Europe. *Journal of Hydrology* **335**, 37-54.

Lowe L, Nathan RJ, Morden R (2005) Assessing the impact of farm dams on streamflows; Part II: regional characterisation *Australian Journal of Water Resources* **9**, 13-26.

Macfarlane C, Arndt SK, Livesley SJ, Edgar AC, White DA, Adams MA, Eamus D (2007) Estimation of leaf area index in eucalypt forest with vertical foliage, using cover and fullframe fisheye photography. *Forest Ecology and Management* **242**, 756-763.

McJannet DL, Webster I, Stenson M, Sherman BS (2008) 'Estimating open water evaporation for the Murray-Darling Basin.' CSIRO, Canberra.

McVicar TR, Jupp DLB (1999) Estimating one-time-of-day meteorological data from standard daily data as inputs to thermal remote sensing based energy balance models. *Agricultural and Forest Meteorology* **96**, 219-238.

McVicar TR, Van Niel TG, Li LT, Roderick ML, Rayner DP, Ricciardulli L, Donohue RJ (2008) Wind speed climatology and trends for Australia, 1975-2006: capturing the stilling phenomenon and comparison with near-surface reanalysis output. *Geophysical Research Letters* **35**.

Monsi M, Saeki T (1953) Über den Lichtfactor in den Pflanzengesellschaften und seine Bedeutung für die Stoffproduktion. *Japanese Journal of Botany* **14**, 22-52.

Monteith JL (1965) Evaporation and environment *Symposia of the Society for Experimental Biology* **19**, 205-224.

Moore RJ (2007) The PDM rainfall-runoff model. *Hydrology and Earth System Sciences* **11**, 483-499.

Morton FI (1983) Operational estimates of areal evapotranspiration and their significance to the science and practice of hydrology *Journal of Hydrology* **66**, 1-76.

Murakami S (2006) A proposal for a new forest canopy interception mechanism: Splash droplet evaporation. *Journal of Hydrology* **319**, 72-82.

Mutziger AJ, Burt CM, Howes DJ, Allen RG (2005) Comparison of measured and FAO-56 modeled evaporation from bare soil. *Journal of irrigation and drainage engineering* **131**, 59-72

Owe M, De Jeu R, Walker J (2001) A methodology for surface soil moisture and vegetation opticaldepth retrieval using the microwave polarization difference index. *IEEE Transactions on Geoscience and Remote Sensing* **39**, 1643-1654.

Prata A (1996) A new long-wave formula for estimating downward clear-sky radiation at the surface. *Quarterly Journal of the Royal Meteorological Society* **122**, 1127-1151.

Priestley CHB, Taylor RJ (1972) On the assessment of surface heat flux and evaporation using large-scale parameters *Monthly Weather Review* **100** 81-92.

Raupach MR (1991) Vegetation-Atmosphere Interaction in Homogeneous and Heterogeneous Terrain: Some Implications of Mixed-Layer Dynamics. *Vegetatio* **91**, 105-120.

Raupach MR, Briggs PR, Haverd V, King EA, Paget M, Trudinger CM (2008) 'Australian Water Availability Project (AWAP) CSIRO Marine and Atmospheric Research Component: Final Report for Phase 3.' CSIRO, Canberra, Australia.

Raupach MR, Kirby JM, Barrett DJ, Briggs PR, Lu H (2001) 'Balances of Water, Carbon, Nitrogen and Phosphorus in Australian Landscapes: (2) Model Formulation and Testing.' CSIRO, Canberra, Australia.

Rawls WJ, Ahuja LR, Brakensiek DL, Shirmohammadi A (1992) Infiltration and soil water movement. In 'Handbook of Hydrology '. (Ed. DR Maidment) pp. 5.1-5.51. (McGraw-Hill

Reggiani P, Sivapalan M, Hassanizadeh SM (1998) A unifying framework for watershed thermodynamics: balance equations for mass, momentum, energy and entropy, and the second law of thermodynamics. *Advances in Water Resources* **22**, 367-398.

Reich PB, Walters MB, Ellsworth DS (1997) From tropics to tundra: Global convergence in plant functioning. *Proceedings of the National Academy of Sciences* **94**, 13730-13734.

Reich PB, Wright IJ, Cavender-Bares J, Craine JM (2003) The Evolution of Plant Functional Variation: Traits, Spectra, and Strategies. *International Journal of Plant Sciences* **164**, S143-S164.

Richards JH, Caldwell MM (1987) Hydraulic lift: substantial nocturnal water transport between soil layers by Artemisia tridentata roots. *Oecologia* **73**, 486-489.

Ritchie JT (1972) Model for predicting evaporation from a row crop with incomplete cover. *Water Resources Research* **8**, 1204-1213.

Roderick M, Hobbins M, Farquhar G (2009) Pan evaporation trends and the terrestrial water balance. I. Principles and Observations. *Geography Compass* **3**, 746-760.

Ross J (1981) 'The radiation regime and architecture of plant stands.' (Dr W Junk Publishers: The Hague, Netherlands)

Schellekens J, Scatena FN, Bruijnzeel LA, Wickel AJ (1999) Modelling rainfall interception by a lowland tropical rain forest in northeastern Puerto Rico. *Journal of Hydrology* **225**, 168-184.

Schulze ED, Turner NC, Nicolle D, Schumacher J (2006) Species differences in carbon isotope ratios, specific leaf area and nitrogen concentrations in leaves of Eucalyptus growing in a common garden compared with along an aridity gradient. *Physiologia Plantarum* **127**, 434-444.

Schymanski SJ, Roderick ML, Sivapalan M, Hutley LB, Beringer J (2008) A canopy-scale test of the optimal water-use hypothesis. *Plant, Cell & Environment* **31**, 97-111.

Shuttleworth W, Wallace J (2007) Evaporation from sparse crops-an energy combination theory. *Quarterly Journal of the Royal Meteorological Society* **111**, 839-855.

Shuttleworth WJ (1992) Evaporation. In 'Handbook of Hydrology '. (Ed. DR Maidment) pp. 4.1-4.53. (McGraw-Hill

Sridhar V, Elliott RL (2002) On the development of a simple downwelling longwave radiation scheme. *Agricultural and Forest Meteorology* **112**, 237-243.
Stagnitti F, Parlange JY, Rose CW (1989) Hydrology of a small wet catchment. *Hydrological Processes* **3**, 137-150.
Thom AS (1975) 3. Momentum, Mass and Heat Exchange of Plant Communities. *Vegetation and the atmosphere: principles*, 57.
Tuzet A, Perrier A, Leuning R (2003) A coupled model of stomatal conductance, photosynthesis and transpiration. *Plant, Cell & Environment* **26**, 1097-1116.
Tyree MT (1999) Water relations of plants. In 'Ecohydrology'. (Routledge: London, UK)
Van der Tol C, Gash JHC, Grant SJ, McNeil DD, Robinson M (2003) Average wet canopy evaporation for a Sitka spruce forest derived using the eddy correlation-energy balance technique. *Journal of Hydrology* **276**, 12-19.
Van Dijk AIJM (2009) Climate and terrain factors explaining streamflow response and recession in Australian catchments. *Hydrology and Earth System Sciences* **14**, 159-169.
Van Dijk AIJM (2010) Selection of an appropriately simple storm runoff model. *Hydrology and Earth Systems Sciences* **14**, 447-458.
Van Dijk AIJM, Bruijnzeel LA (2001a) Modelling rainfall interception by vegetation of variable density using an adapted analytical model. Part 1. Model description. *Journal of Hydrology* **247**, 230-238.
Van Dijk AIJM, Bruijnzeel LA (2001b) Modelling rainfall interception by vegetation of variable density using an adapted analytical model. Part 2. Model validation for a tropical upland mixed cropping system. *Journal of Hydrology* **247**, 239-262.
Van Dijk AIJM, Guerschman JP, Warren GA (2010a) Satellite mapping of areas evaporating river and groundwater flows In 'Proceedings of the Geophysical Research Abstracts'. 12 pp. 2010-7847. (European Geophysical Union)
Van Dijk AIJM, Marvanek S (2010) 'Derivation of a simplified soil drainage model. AWRA background paper 2010/1.' WIRADA / CSIRO Water for a Healthy Country Flagship, Canberra.
Van Dijk AIJM, Renzullo LJ (2009) Evaluation of alternative model-data fusion approaches in retrospective water balance estimation across Australia In 'Proceedings of the 18th World IMACS Congress and MODSIM09 International Congress on Modelling and Simulation'. Cairns, Australia.
Van Dijk AIJM, Warren GA (2010) 'Estimation of AWRA-L model land cover parameters from satellite observations. AWRA background paper 2010/3.' WIRADA / CSIRO Water for a Healthy Country Flagship, Canberra.
Van Dijk AIJM, Warren GA, Doubkova M (2010b) 'A simple albedo model derived from satellite observations. AWRA background paper 2010/2.' WIRADA / CSIRO Water for a Healthy Country Flagship, Canberra.
Wallace J, McJannet D (2006) On interception modelling of a lowland coastal rainforest in northern Queensland, Australia. *Journal of Hydrology* **329**, 477-488.
Wan Z (2008) New refinements and validation of the MODIS Land-Surface Temperature/Emissivity products. *Remote Sensing of Environment* **112**, 59-74.
Wright IJ, Reich PB, Westoby M, Ackerly DD, Baruch Z, Bongers F, Cavender-Bares J, Chapin T, Cornelissen JHC, Diemer M, Flexas J, Garnier E, Groom PK, Gulias J, Hikosaka K, Lamont BB, Lee T, Lee W, Lusk C, Midgley JJ, Navas M-L, Niinemets U, Oleksyn J, Osada N, Poorter H, Poot P, Prior L, Pyankov VI, Roumet C, Thomas SC, Tjoelker MG, Veneklaas EJ, Villar R (2004) The worldwide leaf economics spectrum. *Nature* **428**, 821-827.
Zou CB, Barnes PW, Archer S, McMurtry CR (2005) Soil moisture redistribution as a mechanism of facilitation in savanna tree–shrub clusters. *Oecologia* **145**, 32-40.

APPENDIX A. DERIVATION OF EVAPORATION EQUATIONS

A.1. Introduction

Common approaches to constraining the water balance by coupling to the energy balance tend to either (1) directly use meteorological variables in a surface model (normally a version of the Penman-Monteith combination equation; Monteith 1965) that directly couples energy and water fluxes; (2) define a potential evaporation or evapotranspiration (PET; the hypothetical evaporation rate that would occur under ambient meteorological conditions[10]) and scale this depending on water availability. Both require estimation of the radiation balance; their main difference is in the description of the coupling between the surface and the atmospheric boundary layer.

Penman-Monteith (P-M) type schemas are most common in land surface schemes and suitable for short time steps (e.g. sub-daily) but require information on vegetation roughness and wind speed. PET based approaches make simplifying assumptions about the interaction between the surface and the atmospheric boundary layer and are common in water resources applications. The preference for this approach may be because pre-calculated PET data are often available or at least only needs to be calculated once; because it may be sufficiently accurate given other uncertainties (e.g. in rainfall); and because the additional atmospheric humidity and wind speed data needed are often not available. A combination of the two approaches is followed in AWRA-L, which allows this coupling to be described where the necessary input data is available, but allows simplifying assumptions to be used where they are not.

One of the PET formulations commonly used is that of Priestley and Taylor (1972) (P-T). It has been argued that the P-T approach has a sound physical basis due to the feedback between surface water and energy fluxes and the dynamic lower atmosphere (the convective boundary layer, CBL). It was used in the National Land and Water Resources Audit (Raupach *et al.* 2001), the Murray-Darling Basin Sustainable Yields project (Guerschman *et al.* 2008; Kirby *et al.* 2008) and the Australian Water Availability Project (McJannet *et al.* 2008; Raupach *et al.* 2008; King *et al.* in press).

Based on theoretical arguments P-T PET should provide a valid estimate of actual evaporation over larger (e.g. >10 km) well-watered areas. Uncertainty in the order of ±5% can be expected due to assumptions that are made about the boundary layer (Brutsaert and Stricker 1979; Stagnitti *et al.* 1989 ; Raupach 1991; Hobbins *et al.* 2001). In particular the underlying assumptions about spatial variability in surface roughness, entrainment of air from above the convective boundary layer, and lateral advection of energy may become troublesome.

These issues may not affect estimated actual evaporation rates much when water rather than energy is limiting evaporation. They may be more problematic when evaporation occurs from moist surfaces and is limited by available energy. In such circumstances, evaporation rates may

[10] 'hypothetical' because the atmospheric variables used in calculation (such as air temperature) are directly affected by the actual evaporation rate, which causes a circular logic (that is, if the evaporation indeed were to occur, potential ET would change as a consequence) *except* for situations where actual evaporation and PET are equal. Depending on the formulation, PET may still provide a reasonable estimate of the upper limit to evaporation, however.

be greater than P-T PET because of lateral energy advection (in the form of dry and/or warm air) or greater entrainment of dry air from above into the CBL.

To allow for assumptions or observations to quantify this effect, an analytical and empirical comparison between the P-M and P-T formulations was made and an equation to estimate an 'aerodynamic correction factor' (k_α) developed.

A.2. Basic definitions and equations

Evapotranspiration

Below the basic equations and variables are provided that are the basis for the ET modelling approach follow. Firstly, the P-M big leaf equation is given by (Monteith 1965)[11]:

$$E = \left(\frac{10^3 \Delta t}{\lambda \rho_w}\right) \frac{\Delta A_n + \rho_a c_p D g_a}{\Delta + \gamma\left(1 + g_a / g_S\right)} \qquad [A\text{-}1]$$

where E is daily evaporation rate (in mm d^{-1}), 10^3 converts from m to mm, Δt is the length of the interval considered (86400 s for a day), λ the latent heat of evaporation (converting from energy flux to mass flux; ~ $2.5 \cdot 10^9$ J kg^{-1}), ρ_w the density of water (kg m^{-3}), Δ the saturated vapour pressure–temperature gradient at ambient temperature (Pa K^{-1}), γ the psychometric 'constant' (ca. 66 Pa K^{-1}), R_n net radiation energy (W m^{-1}), ρ_a the density of air (kg m^{-3}), c_p the specific heat of air (J kg^{-1} K^{-1}) at ambient pressure and water content, D the vapour pressure deficit (Pa), g_a the aerodynamic conductance (m s^{-1}), and g_s the surface conductance (m s^{-1}).

The variables λ, Δ, γ, ρ_a, c_p and D are all functions of air temperature and/or vapour pressure, and are defined further below. The method to calculate aerodynamic conductance g_a will also be explained.

The P-M equation will be compared to the P-T approximation of potential ET (E_{0PT} in mm d^{-1}), which is given by:

$$E_{0PT} = \left(\frac{10^3 \Delta t}{\lambda \rho_w}\right) \frac{\Delta}{\Delta + \gamma} \alpha A_n \qquad [A\text{-}2]$$

where α is an empirical factor with an estimated value of 1.26 (Priestley and Taylor 1972) although later authors have suggested values up to 1.32 (see Hobbins *et al.* 2001), whereas under conducive atmospheric conditions (e.g. strong wind, dry air, energy advection) values greater than 1.7 can occur (Section 3.8).

Thermodynamic equations

Thermodynamic equations are used to estimate the variables D, γ and ρ_a. They depend on vapour pressure (e in Pa), air temperature (T in °C) and, for the last two cases, air pressure (p in Pa). Vapour pressure deficit D is defined as:

$$D = e_s - e \qquad [A\text{-}3]$$

where e_s is vapour pressure at saturation point and e is actual vapour pressure (both in Pa).

$$c_p = c_{pd}\left(\frac{p - e}{p}\right) + c_{pv} \frac{m_{H_2O}}{m_{air}} \frac{e}{p} \qquad [A\text{-}4]$$

[11] For the benefit of readers familiar with the literature the most commonly used notation is adhered to here. The symbols used often vary from those used in the body text and are not in the List of Symbols.

where c_{pd} and c_{pv} are the specific heat of dry air (1005 J kg^{-1} K^{-1}) and vapour (1870 J kg^{-1} K^{-1}), respectively, m_{H2O} (18.016 u or g mol^{-1}) and m_{air} (28.966 u) are the molecular weights of water and dry air, respectively, and p is air pressure (Pa).

$$\gamma = \frac{m_{air} c_p p}{m_{H_2O} \lambda} \quad \text{[A-5]}$$

Finally, the ideal gas law states that:

$$\rho_a = \frac{p}{R_{air}(T + 273.16)} \quad \text{[A-6]}$$

where the 273.16 °C is to convert from T in °C to absolute temperature (in K), and

$$R_{air} = \left(\frac{p - e}{p}\right) R_{dry} + \frac{e}{p} R_{H2O} \quad \text{[A-7]}$$

and R_{dry} (287.058 J kg^{-1} K^{-1}) and R_{H2O} (461.5 J kg^{-1} K^{-1}) are the gas constants for dry air and water vapour, respectively.

Finally, approximation equations are required for e_s, Δ and λ and are, following Shuttleworth (1992):

$$e_s = 610.8 \exp\left(\frac{17.27T}{237.3 + T}\right) \quad \text{[A-8]}$$

with e_s in Pa and T in °C;

$$\Delta = \frac{de_s}{dT} = \frac{4098 e_s}{(237.3 + T)^2} \quad \text{[A-9]}$$

$$\lambda = 2.501 \cdot 10^6 - 2361 \cdot T \quad \text{[A-10]}$$

where λ has units of J kg^{-1}.

$$\rho_w = 1000 - \left(\frac{T - 4}{119.1}\right) - \left(\frac{T - 4}{12.04}\right)^2 + \left(\frac{T - 4}{32.12}\right)^3 \quad \text{[A-11]}$$

where ρ_w has units of kg m^{-3}.

$$f_{RH} = \frac{e}{e_s} \quad \text{[A-12]}$$

A.3. Reformulation of the Penman-Monteith equation

Rearrangement

Below the P-M equation is manipulated and simplified with the following objectives:

1. Allow the use of a simplification similar to that of Priestley and Taylor where wind speed observations are not available.
2. Derive approximation equations to estimate terms combining variables that are only dependent on air pressure, temperature and vapour pressure.
3. Derive simplifications for use where air and vapour pressure data are also not available.

To this end, Eq. [A-1] is re-arranged as follows:

$$E = \left(\frac{10^3 \Delta t}{\lambda \rho_w}\right) \frac{\Delta}{\Delta + \gamma} \left(1 + \frac{f_{day} \rho_a c_p D}{\Delta} \frac{g_a}{A_n}\right) \left(\frac{1}{1 + \left(\frac{\gamma}{\Delta + \gamma}\right) \frac{g_a}{g_s}}\right) A_n \quad \text{[A-13]}$$

a **b** **c** **d** **e**

The fraction of daylight hours f_{day} is introduced on the assumption that evaporation occurs during daylight hours only. The above equation can be re-expressed as follows:

$$E = f_c E_0 = f_c \left[c_{RE} \left(\frac{1}{1 + \varepsilon} \right) f_\alpha \right] A_n \quad \text{[A-14]}$$

where f_c is similar to a crop factor, E_0 potential ET, c_{RE} a unit conversion that converts from sensible heat flux (W m^{-2}) to evaporation (mm d^{-1}), $\varepsilon = \gamma/\Delta$, and f_α equivalent to the P-T coefficient, representing the terms a–d as follows:

$$c_{RE} = \frac{10^3 \Delta t}{\lambda \rho_w} \quad \textbf{(a)} \quad \text{[A-15]}$$

$$\frac{1}{1 + \varepsilon} = \frac{\Delta}{\Delta + \gamma} \quad \textbf{(b)} \quad \text{[A-16]}$$

$$f_\alpha = 1 + \frac{C_{aero} g_a}{A_n} \quad \textbf{(c)} \quad \text{[A-17]}$$

$$f_c = \left[1 + \left(\frac{\varepsilon}{1 + \varepsilon} \right) \frac{g_a}{g_s} \right]^{-1} \quad \textbf{(d)} \quad \text{[A-18]}$$

and C_{aero} (J m^{-3}) a conversion coefficient expressing efficiency of aerodynamic energy use:

$$C_{aero} = \frac{f_{day} \rho_a c_p D}{\Delta} \quad \text{[A-19]}$$

Simplifications

To avoid the several variables, constants and approximation equations involved in calculation of c_{RE} and C_{aero}, they were evaluated and simplified where possible. This was done for air temperatures between 0 and 50 °C and for relative humidity of 0 to 100%. New empirical equations were found to replace combinations of multiple empirical equations, and constants were inserted. This allowed the following simplifications:

$$c_{RE} = 0.03449 + 4.27 \cdot 10^{-5} T$$

This approximation is within 0.2% accurate for the entire temperature and humidity range. It produces values varying between 0.0345 mm d^{-1} per W m^{-2} at 0°C to 0.0367 mm d^{-1} per W m^{-2} at 50°C (i.e a range of ±3% of the average)

$$\varepsilon = \frac{\gamma}{\Delta} = \frac{m_{air} p \left[c_{pd} \left(\frac{p-e}{p} \right) + c_{pv} \frac{m_{H_2O}}{m_{air}} \frac{e}{p} \right]}{m_{H_2O} \left(2.501 \cdot 10^6 - 2361T \right)} \frac{(237.3+T)^2}{4098 e_s} \qquad \text{[A-20]}$$

Inserting values for all constants and finding a simpler function of T produced:

$$\varepsilon = 1.40 \cdot 10^{-3} \left[\left(\frac{T}{187} \right)^2 + \frac{T}{107} + 1 \right] \left(\frac{6.36p + e}{e_s} \right) \qquad \text{[A-21]}$$

This approximation was accurate within 0.01% across the range of air temperature and humidity considered here. It produces values from 1.42 at 0 °C to 0.11 at 50 °C (that is, the vapour pressure dependency is very small).

Inserting in all (approximation) equations in the expression for C_{aero} (Eq. [A-19]) produces:

$$\begin{aligned} C_{aero} &= f_{day} \frac{p c_p (e_s - e)}{R_{air} (T + 273.15) \Delta} \\ &= \frac{p \left[c_{pd} \left(\frac{p-e}{p} \right) + c_{pv} \frac{m_{H_2O}}{m_{air}} \frac{e}{p} \right]}{\left[\left(\frac{p-e}{p} \right) R_{dry} + \frac{e}{p} R_{H2O} \right] (T + 273.15)} \frac{(237.3+T)^2 (e_s - e)}{4098 e_s} \end{aligned} \qquad \text{[A-22]}$$

This can be simplified by inserting the constants and simplifying the approximation functions:

$$C_{aero} = f_{day} 0.176 \left(1 + \frac{T}{209.1} \right) (p - 0.417e) \left(1 - \frac{e}{e_s} \right) \qquad \text{[A-23]}$$

This is accurate within 0.07% for the tested range. The resulting value of C_{aero} is almost proportionally dependent on relative humidity (reducing to zero when for f_{RH}=100%), and varies by ca. 8–11% over the tested temperature range. A value for f_{RH}=70% and air temperature of 25°C is 5710 J m^{-3}.

A.4. Aerodynamic conductance

Aerodynamic conductance g_a can be estimated as (Brutsaert 1982):

$$g_a = f_{uz} u_z = \frac{k_2}{\left[\ln\left(\frac{z-d}{z_{0m}}\right) - \Psi_M\right]\left[\ln\left(\frac{z-d}{z_{0v}}\right) - \Psi_H\right]} u_z \qquad \text{[A-24]}$$

where u_z (m s^{-1}) is wind speed measured at a reference height z (m) above the ground surface and f_{uz} is a local fraction that is a function of the Von Kármán constant (0.41), the displacement height d, z_{0m} and z_{0v} (both in m) the roughness lengths for momentum and vapour transport, respectively, and Ψ_M and Ψ_H the Monin-Obukhov stability corrections for momentum and vapour, respectively. The stability corrections are only necessary under non-neutral atmospheric conditions (low wind speed, instable atmosphere). Because these corrections are not straightforward and because there are far greater uncertainties in the estimation of ET in general and aerodynamic conductance in particular, it is assumed that $\Psi_M=\Psi_H=0$.

Following Thom (1975) d, z_{0m}, and z_{0v} can be estimated as:

$$d = 0.67h$$
$$z_{0m} = 0.123h \qquad \text{[A-25abc]}$$
$$z_{0v} = 0.1 z_{0m}$$

If wind speed measurements at 2 m height in climate stations (u_2) are available, for these data to be used over other vegetation types wind speed at a height in the atmosphere nearly unaffected by surface roughness needs to be calculated using the logarithmic wind profile:

$$u_z = \frac{u^*}{k} \ln\left(\frac{z-d}{z_{0m}}\right) \qquad \text{[A-26]}$$

where u^* is the friction velocity. It follows that the relationship between u_2 and wind speed higher in the atmosphere u_z is defined by:

$$u_z = u_2 \ln\left(\frac{z-d}{z_{0m}}\right) \Big/ \ln\left(\frac{2-d}{z_{0m}}\right) \qquad \text{[A-27]}$$

Assuming the climate station and its surroundings have grass with an FAO-56 reference crop height (0.12 m), the estimated wind speed at 100 m height becomes:

$$u_z = u_2 \ln\left(\frac{100 - 0.67 \cdot 0.12}{0.123 \cdot 0.12}\right) \Big/ \ln\left(\frac{2 - 0.67 \cdot 0.12}{0.123 \cdot 0.12}\right) = 1.81 u_2 \qquad \text{[A-28]}$$

This can be combined with Eq. [A-24] as follows:

$$f_{u2} = \frac{k^2}{\ln\left(\frac{100-d}{z_{0m}}\right)\left[\ln\left(\frac{100-d}{z_{0m}}\right)+\ln\left(\frac{z_{0m}}{z_{0v}}\right)\right]}1.81 \qquad [A\text{-}29]$$

$$= \frac{0.305}{f(h)\left(f(h)+2.3\right)}$$

where

$$f(h) = \ln\left(\frac{813}{h} - 5.45\right) \qquad [A\text{-}30]$$

APPENDIX B. MODEL CODE

B.1. Time step model

AWRA Landscape model version 0.5 exists in several platforms. The original reference implementation, also used to produce simulations for the model evaluation report (Report 4), was written as a MATLAB™ script. The dynamic part of the model (that is, the code executed at each time step to evolve the model) is reproduced below. Model pre-processing of the input data and the overall workflow execution are done by other scripts that available upon request.

Note that parameter and variable references may occasionally vary from those used in this report. Further note that the comments below can vary somewhat from the comments in the original code, e.g. due to changes in the section numbering after report revision. The section numbering below applies to the current report.

```
function [state,out]=timestep_05(in,state,par)

% Australian Water Resources Assessment Landscape (AWRA-L) model
% This script contains the AWRA-L time step model
%
% Full documentation is found in the technical reference:
%
% Van Dijk, A.I.J.M. (2010) The Australian water resources assessment system.
% Technical Report 3. Landscape Model (version 0.5) Technical Description
% WIRADA Technical Report, CSIRO Water for a Healthy Country Flagship, Canberra.
%
% The section references below refer to the sections in the above report.

% ASSIGN STATE VARIABLES
S0          =   state.S0;
Ss          =   state.Ss;
Sd          =   state.Sd;
Sg          =   state.Sg;
Sr          =   state.Sr;
Mleaf       =   state.Mleaf;

% ASSIGN INPUT VARIABLES
Pg          =   in.Pg;
Rg          =   in.Rg;
Ta          =   in.Ta;
pe          =   in.pe;
pair        =   in.pair;
u2          =   in.u2;

% ASSIGN PARAMETERS
Nhru        =   par.Nhru;
Fhru        =   par.Fhru;
SLA         =   par.SLA;
LAIref      =   par.LAIref;
Sgref       =   par.Sgref;
S0FC        =   par.S0FC;
SsFC        =   par.SsFC;
SdFC        =   par.SdFC;
fday        =   par.fday;
Vc          =   par.Vc;
alb_dry     =   par.alb_dry;
alb_wet     =   par.alb_wet;
w0ref_alb   =   par.w0ref_alb;
Gfrac_max   =   par.Gfrac_max;
fvegref_G   =   par.fvegref_G;
hveg        =   par.hveg;
```

```
Us0          =   par.Us0;
Ud0          =   par.Ud0;
wslimU       =   par.wslimU;
wdlimU       =   par.wdlimU;
cGsmax       =   par.cGsmax;
FsoilEmax    =   par.FsoilEmax;
w0limE       =   par.w0limE;
FwaterE      =   par.FwaterE;
S_sls        =   par.S_sls;
ER_frac_ref  =   par.ER_frac_ref;
InitLoss     =   par.InitLoss;
PrefR        =   par.PrefR;
FdrainFC     =   par.FdrainFC;
beta         =   par.beta;
Fgw_conn     =   par.Fgw_conn;
K_gw         =   par.K_gw;
K_rout       =   par.K_rout;
LAImax       =   par.LAImax;
Tgrow        =   par.Tgrow;
Tsenc        =   par.Tsenc;

% diagnostic equations
LAI          =   SLA.*Mleaf;    % (5.3)
fveg         =   1 - exp(-LAI./LAIref) ;     % (5.3)
fsoil        =   1 - fveg;
w0           =   S0./S0FC;     % (2.2)
ws           =   Ss./SsFC;     % (2.2)
wd           =   Sd./SdFC;     % (2.2)

% Spatialise catchment fractions (3.8)
fwater=[];fsat=[]; Sghru=[];
for i=1:par.Nhru
    fwater   =   [fwater; min(0.005,0.007.*Sr.^0.75)];
    fsat     =   [fsat; min(1,max(min(0.005,0.007.*Sr.^0.75),Sg./Sgref))];
    Sghru    =   [Sghru; [Sg]];
end

% CALCULATION OF PET
% Conversions and coefficients (3.2)
pes          =   610.8.*exp(17.27.*Ta./(237.3+Ta));
fRH          =   pe./pes;
cRE          =   0.03449+4.27e-5.*Ta;
Caero        =   fday.*0.176.*(1+Ta./209.1).*(pair-0.417.*pe).*(1-fRH);
keps         =   1.4e-3.*((Ta./187).^2+Ta./107+1).*(6.36.*pair+pe)./pes;
Rgeff        =   Rg./fday;
% shortwave radiation balance (3.4)
alb_veg      =   0.452.*Vc;
alb_soil     =   alb_wet+(alb_dry-alb_wet).*exp(-w0./w0ref_alb);
alb          =   fveg.*alb_veg+fsoil.*alb_soil;
RSn          =   (1-alb).*Rgeff;
% longwave radiation balance
StefBolz     =   5.67e-8;
Tkelv        =   Ta+273.16;
RLin         =   (0.65.*(pe./Tkelv).^0.14).*StefBolz.*Tkelv.^4;     % (3.5)
RLout        =   1.*StefBolz.*Tkelv.^4;      % (3.6)
RLn          =   RLin-RLout;
fGR          =   Gfrac_max.*(1-exp(-fsoil./fvegref_G));     % (3.7)
Rneff        =   (RSn+RLn).*(1-fGR);
% Aerodynamic conductance (3.9)
fh           =   log(813./hveg-5.45);
ku2          =   0.305./(fh.*(fh+2.3));
ga           =   ku2.*u2;
%  Potential evaporation (3.8)
kalpha       =   1+Caero.*ga./Rneff;
E0           =   cRE.*(1./(1+keps)).*kalpha.*Rneff.*fday;

% CALCULATION OF ET FLUXES AND ROOT WATER UPTAKE
% Root water uptake constraint (4.4)
Usmax        =   Us0.*min(1,ws./wslimU);
Udmax        =   Ud0.*min(1,wd./wdlimU);
U0           =   max(Usmax,Udmax);
% Maximum transpiration (4.3)
Gsmax        =   cGsmax.*Vc;
gs           =   fveg.*Gsmax;
ft           =   1./(1+(keps./(1+keps)).*ga./gs);
Etmax        =   ft.*E0;
% Actual transpiration (4.1)
Et           =   min(U0, Etmax);
```

```
% Root water uptake distribution (2.4)
Us          =   min( (Usmax./(Usmax+Udmax)).*Et, Ss-1e-2 ) ;
Ud          =   min( (Udmax./(Usmax+Udmax)).*Et, Sd-1e-2 ) ;
Et          =   Us + Ud;      % to ensure mass balance
% Soil evaporation (4.5);
fsoilE      =   FsoilEmax.*min(1,w0./w0limE) ;
Es          =   (1-fsat).*fsoilE.*( E0-Et ) ;
% Groundwater evaporation (4.6);
Eg          =   (fsat-fwater).*FsoilEmax.*( E0-Et ) ;
% Open water evaporation (4.7);
Er          =   fwater.*FwaterE.*( E0-Et ) ;
% Rainfall interception evaporation (4.2)
Sveg        =   S_sls.*LAI;
fER         =   ER_frac_ref.*fveg;
Pwet        =   -log(1-fER./fveg).*Sveg./fER;
Ei          =   (Pg<Pwet).*fveg.*Pg+(Pg>=Pwet).*(fveg.*Pwet+fER.*(Pg-Pwet));

% CALCULATION OF WATER BALANCES
% soil surface water fluxes (2.3)
Pn          =   max(0, Pg - Ei - InitLoss)  ;
Rhof        =   (1-fsat).*( Pn./(Pn+PrefR) ).*Pn  ;
Rsof        =   fsat .*Pn ;
QR          =   Rhof + Rsof ;
I           =   Pg - Ei - QR  ;
% SOIL WATER BALANCES (2.1 inc drainage 2.5)
% Topsoil (S0)
S0          =   S0  + I - Es  ;
SzFC        =   S0FC;
Sz          =   S0;
wz          =   max(1e-2,Sz)./SzFC;
fD          =  (wz>1).*max(FdrainFC,1-1./wz) + (wz<=1).*FdrainFC.*exp(beta.*(wz-1) );
Dz          =   min(fD.*Sz,Sz-1e-2);
D0          =   Dz;
S0          =   S0  - D0 ;
% Shallow soil(Ss)
Ss          =   Ss  + D0 -  Us;
SzFC        =   SsFC;
Sz          =   Ss;
wz          =   max(1e-2,Sz)./SzFC;
fD          =  (wz>1).*max(FdrainFC,1-1./wz) + (wz<=1).*FdrainFC.*exp(beta.*(wz-1) );
Dz          =   min(fD.*Sz,Sz-1e-2);
Ds          =   Dz;
Ss          =   Ss  - Ds ;
% Deep soil (Sd) (inc capillary rise 2.7)
Sd          =   Sd  + Ds -  Ud;
SzFC        =   SdFC;
Sz          =   Sd;
wz          =   max(1e-2,Sz)./SzFC;
fD          =  (wz>1).*max(FdrainFC,1-1./wz) + (wz<=1).*FdrainFC.*exp(beta.*(wz-1) );
Dz          =   min(fD.*Sz,Sz-1e-2);
Dd          =   Dz;
Sd          =   Sd  - Dd;
Y           =   min(Fgw_conn.*max(0,wdlimU.*SdFC-Sd),Sghru);
Sd          =   Sd + Y;

% CATCHMENT WATER BALANCE
% Groundwater store water balance (Sg) (2.6)
NetGf       =   sum(Fhru.*(Dd - Eg - Y));
Sg          =   Sg + NetGf;
Qg          =   min(Sg, (1-exp(-K_gw)).*Sg) ;
Sg          =   Sg - Qg;
% Surface water store water balance (Sr) (2.8)
Sr          =   Sr  +  sum(Fhru.*(QR - Er) ) + Qg ;
Qtot        =   min(Sr, (1-exp(-K_rout)).*Sr) ;
Sr          =   Sr  - Qtot;

% VEGETATION ADJUSTMENT (5)
fveq        =   (1./max((E0./U0)-1,1e-3)).*(keps./(1+keps)).*(ga./Gsmax);
fvmax       =   1-exp(-LAImax./LAIref);
fveq        =   min(fveq,fvmax);
dMleaf      =   -log(1-fveq).*LAIref./SLA-Mleaf ;
Mleafnet    =   (dMleaf>0).*min(dMleaf./Tgrow,MaxGrow) +(dMleaf<0).*dMleaf./Tsenc;
Mleaf       =   Mleaf + Mleafnet;

% Updating diagnostics
LAI         =   SLA.*Mleaf;                 % (5.3)
fveg        =   1 - exp(-LAI./LAIref) ;     % (5.3)
fsoil       =   1 - fveg;
```

```
w0          =   S0./S0FC;                   % (2.1)
ws          =   Ss./SsFC;                   % (2.1)
wd          =   Sd./SdFC;                   % (2.1)

% ASSIGN OUTPUT VARIABLES
% fluxes
out.E0      =   sum(Fhru.*E0);
out.Ee      =   sum(Fhru.*(Es + Eg + Er + Ei));
out.Et      =   sum(Fhru.*Et);
out.Ei      =   sum(Fhru.*Ei);
out.Etot    =   out.Et + out.Ee;
out.Qtot    =   Qtot;
out.gwflux  =   NetGf;
% states
out.S0      =   sum(Fhru .* S0);
out.Ss      =   sum(Fhru .* Ss);
out.Sd      =   sum(Fhru .* Sd);
out.Sg      =   Sg;
out.Stot    =   out.S0 + out.Ss + out.Sd + Sg + Sr + sum(Fhru .* Mleaf.*(0.8/0.2);
% NOTE: 0.8 because wet leaf biomass is assumed to consist of 80% water
out.Mleaf   =   sum(Fhru .* Mleaf);
out.LAI     =   sum(Fhru .* LAI);
out.fveg    =   sum(Fhru .* fveg) ;
out.fveq    =   sum(Fhru .* fveq);
% synthetic satellite products
out.albedo  =   sum(Fhru .* alb ) ;
out.EVI     =   sum(Fhru .* (Vc.*fveg+0.07) ) ;
% NOTE 0.07 is assumed EVI for bare soil
out.fsat    =   sum(Fhru .* fsat);
out.wunsat  =   sum(Fhru .* w0);

% ASSIGN STATE VARIABLES
state.S0    =   S0;
state.Ss    =   Ss;
state.Sd    =   Sd;
state.Sg    =   Sg;
state.Sr    =   Sr;
state.Mleaf =   Mleaf;

%=========EoF=========
```

B.2. Parameter values

Notations used in the model code reproduced vary from those used in the model description in AWRA Technical Report 3, due to revisions in the latter after model development and evaluation. This will be addressed in future versions. To assist in interpreting the model code, the two notations are compared for all model parameters below. Also listed are the parameter values used for the two HRUs considered in model evaluation (see Technical Report 4 for further details).

Table 2. Parameter settings used in all runs performed for the current evaluation of AWRA version 0.5. All values are default values except those shaded and printed bold (see text). Listed are both the 'model code' notation (used in the MATLAB code for AWRA-L version 0.5), and the 'symbol' notation used in the textual model description. Both can be found in AWRA Technical Report 3.

Code	Symbol	HRU1	HRU2	HRU1: tall, deep-rooted vegetation HRU2: short, shallow-rooted vegetation
alb_dry	α_{dry}	0.26	0.26	dry soil albedo (-)
alb_wet	α_{wet}	0.16	0.16	wet soil albedo (-)
beta	β	4.5	4.5	coefficient describing rate of hydraulic conductivity increase with water content (-)
cGsmax	n/a	0.03	0.03	multiplier to estimate Gsmax from PCI (m s^{-1})
ER_frac_ref	F_{ER0}	0.20	0.05	average ratio of wet canopy evaporation rate and rainfall rate for full canopy cover (-)
Fgw_conn	F_{dg}	1	1	factor describing soil-groundwater connectivity (-)
FsoilEmax	f_{sEmax}	0.2	0.5	maximum soil evaporation fraction (-)
fvegref_G	$F_{S,ref}$	0.15	0.15	reference soil cover fraction that determines the rate of decline in energy loss with increasing canopy cover (-)
FwaterE	F_{OW}	0.7	0.7	open water evaporation scaling factor (-)
Gfrac_max	$F_{loss,max}$	0.3	0.3	maximum fraction of daytime net radiation 'lost' to heat storage when there is no vegetation (-)
hveg	h	10	0.5	vegetation canopy height (m)
InitLoss	I_0	5	5	initial retention capacity (mm)
LAImax	Λ_{max}	8	8	maximum achievable LAI (-)
LAIref	Λ_{ref}	2.5	1.4	reference LAI determining canopy cover (-)
PrefR	P_{ref}	150	150	reference event precipitation for runoff generation (mm d^{-1})
S_sls	s_V	0.1	0.1	canopy storage capacity per unit leaf area (mm)
S0FC	S_{0FC}	30	30	accessible top soil water storage at field capacity (mm)
SdFC	S_{dFC}	1000	1000	accessible deep soil water storage at field capacity (mm)
SsFC	S_{sFC}	200	200	accessible shallow soil water storage at field capacity (mm)
SLA	C_{SLA}	3	10	specific leaf area per unit dry leaf biomass (m^2 kg^{-1})
Tgrow	t_{grow}	1000	150	time constant determining rate of canopy increase (d)
Tsenc	$t_{senesce}$	60	10	time constant determining rate of canopy decrease (d)
Ud0	U_{0d}	4	0	maximum root water uptake from deep soil (mm d^{-1})
Us0	U_{0s}	6	6	maximum root water uptake from shallow soil (mm d^{-1})

Code	Symbol	HRU1	HRU2	HRU1: tall, deep-rooted vegetation HRU2: short, shallow-rooted vegetation
Vc	PCI	0.35	0.65	photosynthetic capacity index
w0limE	w_{0lim}	0.85	0.85	relative top soil water content at which evaporation is reduced (-)
w0ref_alb	$w_{\alpha,ref}$	0.3	0.3	reference value of w_0 describing the relationship between albedo and top soil wetness (-)
wdlimU	w_{dlim}	0.3	0.3	relative deep soil water content at which root uptake is reduced (-)
wslimU	w_{slim}	0.3	0.3	relative shallow soil water content at which root uptake is reduced (-)

.

Contact Us
Phone: 1300 363 400
+61 3 9545 2176
Email: enquiries@csiro.au
Web: www.csiro.au

Your CSIRO

Australia is founding its future on science and innovation. Its national science agency, CSIRO, is a powerhouse of ideas, technologies and skills for building prosperity, growth, health and sustainability. It serves governments, industries, business and communities across the nation.